

synthesize first-stranded cDNAs. The resultant cDNAs were examined by real-time PCR with specific primers for *Photinus* and *Renilla luciferase*. RNA expression levels for *Photinus luciferase* are normalized against those of *Renilla luciferase*, and the ratios of *Photinus luciferase* RNA expression levels in the presence of the si(T9/C10) or si(T11/C12) duplexes are normalized against the ratios obtained in the presence of the siControl duplex. Data are averages of at least three independent determinations. Error bars represent standard deviations.

CONCLUSIONS

The present assay system with wild-type- and mutant-reporter alleles could permit assessment of siRNA duplexes having the potential for specifically inhibiting the expression of the mutant allele without inhibiting the expression of the wild-type allele, and thus contribute to the design and selection of siRNA duplexes suitable for allele-specific gene silencing.

ACKNOWLEDGEMENTS

This work was supported in part by research grants from the Ministry of Health, Labor, and Welfare in Japan and by Promega KK. We would like to thank Dr. H. Tanahashi for providing the pAPP695^{SWE} and pAPP695^{WT} plasmids and Drs. Y. Wang and K. Wada for providing Cos-7 cells. We also thank Y. Tamura, T. Sakai, K. Omi and Dr. A. Hasegawa for their helpful cooperation.

STATEMENT OF COMPETING INTERESTS

Corresponding author has a pending patent on the method of this paper.

LIST OF ABBREVIATIONS

ASP-RNAi; Allele-specific RNA interference
APP; Amyloid precursor protein
TK; Thymidine kinase
UTR; Untranslated region
sAPP; Secreted APP
cAPP; Cellular APP
A β ; Amyloid β

REFERENCES

Cai XD, Golde TE and Younkin SG. 1993. Release of excess amyloid beta protein from a mutant amyloid beta protein precursor. *Science*, 259, 514-516.
Caplen NJ. 2004. Gene therapy progress and prospects. Downregulating gene expression: the impact of RNA interference. *Gene Ther*, 11, 1241-1248.
Chiu YL and Rana TM. 2003. siRNA function in RNAi: a chemical modification analysis. *RNA* 9, 1034-1048.
Citron M, Oltersdorf T, Haass C et al. 1992. Mutation of the beta-amyloid precursor protein in familial Alzheimer's disease increases beta-protein production. *Nature*, 360, 672-674.
Du Q, Thonberg H, Wang J, Wahlestedt C and Liang Z. 2005. A systematic analysis of the silencing effects of an active siRNA at all single-nucleotide mismatched target sites. *Nucleic Acids Res* 33, 1671-1677.
Dykxhoorn DM, Novina CD and Sharp PA. 2003. Killing the messenger: short RNAs that silence gene expression. *Nat Rev Mol Cell Biol*, 4, 457-467.
Goate A, Chartier-Harlin MC, Mullan M et al. 1991. Segregation of a missense mutation in the amyloid precursor protein gene with familial Alzheimer's disease. *Nature*, 349, 704-706.

Hall AH, Wan J, Shaughnessy EE, Ramsay Shaw B and Alexander KA. 2004. RNA interference using boranophosphate siRNAs: structure-activity relationships. *Nucleic Acids Res*, 32, 5991-6000.
Hannon GJ and Rossi JJ. 2004. Unlocking the potential of the human genome with RNA interference. *Nature*, 431, 371-378.
Hohjoh H. 2002. RNA interference (RNAi) induction with various types of synthetic oligonucleotide duplexes in cultured human cells. *FEBS Lett*, 521, 195-199.
Jackson AL, Bartz SR, Schelter J et al. 2003. Expression profiling reveals off-target gene regulation by RNAi. *Nat Biotechnol*, 21, 635-637.
Karagiannis TC and El-Osta A. 2005. RNA interference and potential therapeutic applications of short interfering RNAs. *Cancer Gene Ther*, 12, 787-795.
Lesne S, Docagne F, Gabriel C et al. 2003. Transforming growth factor-beta 1 potentiates amyloid-beta generation in astrocytes and in transgenic mice. *J Biol Chem*, 278, 18408-18418.
Mattson, M. P. (2004). Pathways towards and away from Alzheimer's disease. *Nature* 430, 631-639.
Meister G and Tuschl T. 2004. Mechanisms of gene silencing by double-stranded RNA. *Nature*, 431, 343-349.
Mello CC and Conte D, Jr. 2004. Revealing the world of RNA interference. *Nature*, 431, 338-342.
Mullan M, Crawford F, Axelman K et al. 1992. A pathogenic mutation for probable Alzheimer's disease in the APP gene at the N-terminus of beta-amyloid. *Nat Genet*, 1, 345-347.
Ohnishi Y, Tokunaga K and Hohjoh H. 2005. Influence of assembly of siRNA elements into RNA-induced silencing complex by fork-siRNA duplex carrying nucleotide mismatches at the 3'- or 5'-end of the sense-stranded siRNA element. *Biochem Biophys Res Commun*, 329, 516-521.
Poy MN, Eliasson L, Krutzfeldt J et al. 2004. A pancreatic islet-specific microRNA regulates insulin secretion. *Nature*, 432, 226-230.
Sago N, Omi K, Tamura Y et al. 2004. RNAi induction and activation in mammalian muscle cells where Dicer and eIF2C translation initiation factors are barely expressed. *Biochem Biophys Res Commun*, 319, 50-57.
Suzuki N, Cheung TT, Cai XD et al. 1994. An increased percentage of long amyloid beta protein secreted by familial amyloid beta protein precursor (beta APP717) mutants. *Science*, 264, 1336-1340.
Tanahashi H and Tabira T. 2001. Three novel alternatively spliced isoforms of the human beta-site amyloid precursor protein cleaving enzyme (BACE) and their effect on amyloid beta-peptide production. *Neurosci Lett*, 307, 9-12.
Tang G. 2005. siRNA and miRNA: an insight into RISCs. *Trends Biochem Sci*, 30, 106-114.
Ui-Tei K, Naito Y, Takahashi F et al. 2004. Guidelines for the selection of highly effective siRNA sequences for mammalian and chick RNA interference. *Nucleic Acids Res*, 32, 936-948.
Victor M, Bei Y, Gay F et al. 2002. HAT activity is essential for CBP-1-dependent transcription and differentiation in *Caenorhabditis elegans*. *EMBO Rep*, 3, 50-55.
Wood MJ, Trulzsch B, Abdelgany A and Beeson D. 2003. Therapeutic gene silencing in the nervous system. *Hum Mol Genet*, 12 Spec No 2, R279-284.

Short communication

Gene silencing analyses against *amyloid precursor protein (APP)* gene family by RNA interference

Tokiko Sakai^{a,b}, Hirohiko Hohjoh^{a,*}

^a National Institute of Neuroscience, National Center of Neurology and Psychiatry, 4-1-1 Ogawahigashi, Kodaira, Tokyo 187-8502, Japan

^b Central Research Laboratories, Seikagaku Corporation, Tokyo, Japan

Received 28 March 2006; revised 3 June 2006; accepted 26 June 2006

Abstract

Amyloid precursor protein (APP) and *amyloid precursor-like proteins 1 and 2 (APLP1 and APLP2)* are members of a large gene family. Although APP is known to be the source of the β -amyloid peptides involved in the development of Alzheimer's disease, the normal functions of APP, APLP1 and APLP2 in cells are poorly understood. In this study, we carried out gene silencing analysis by means of RNA interference with synthetic small interfering RNA duplexes targeting the *App*, *Aplp1* and *Aplp2* genes in Neuro2a (N2a) cells, a mouse neuroblastoma cell line. The results demonstrated that cell viability and neurite outgrowth of N2a cells undergoing knockdown of *Aplp1* were significantly reduced, compared with N2a cells undergoing knockdown of either *App* or *Aplp2*.

© 2006 International Federation for Cell Biology. Published by Elsevier Ltd. All rights reserved.

Keywords: RNAi; App; Aplp1; Aplp2; Neuro2a cell; Neurite outgrowth; Viability

1. Introduction

Amyloid precursor protein (APP) is a membrane-spanning glycoprotein expressed in various tissues, including the brain, and is the source of β -amyloid peptides ($A\beta$), which are a key factor in the development of Alzheimer's disease (AD); extracellular deposition of $A\beta$ resulting in the formation of 'senile plaques' often occurring in the brains of AD patients (Turner et al., 2003). In mammals, *amyloid precursor-like protein 1 and 2 (APLP1 and APLP2)* genes, which lack the $A\beta$ region, have also been identified (Wasco et al., 1992; Wasco et al., 1993a,b), thus suggesting that APP, APLP1 and APLP2 are members of a large gene family. The expression profiles of APP and APLP2 are similar, whereas expression of APLP1 appears to be restricted to the nervous system (Lorent et al., 1995; Slunt et al., 1994). Translated APP, APLP1 and APLP2 polypeptides appear to undergo proteolytic processing

by α -, β - and γ -secretase (Eggert et al., 2004; Gu et al., 2001; Li and Sudhof, 2004; Scheinfeld et al., 2002); but, the normal function of the resultant APP, APLP1 and APLP2 in cells remains largely unknown.

In this study, we carried out gene silencing analysis against the *App*, *Aplp1* and *Aplp2* genes by means of RNA interference (RNAi) in Neuro2a (N2a) cells, a mouse neuroblastoma cell line, and investigated the influence of knockdown of these genes.

2. Materials and methods

2.1. Cell culture

Neuro2a cells, a mouse neuroblastoma cell line, were grown at 37 °C in DMEM (Wako) supplemented with 10% fetal bovine serum (Sigma), 100 U/ml penicillin (Invitrogen) and 100 μ g/ml streptomycin (Invitrogen) in a 5% CO₂-humidified chamber.

2.2. Small interfering RNA duplexes

Small interfering RNA (siRNA) duplexes against mouse *App*, *Aplp1*, and *Aplp2* genes were purchased from Ambion. The siRNA ID numbers (Ambion)

* Corresponding author. Tel.: +81 42 341 2711x5951; fax: +81 42 346 1755.
E-mail address: hohjoh@ncnp.go.jp (H. Hohjoh).

were as follows: siApp-1 [60001], siApp-2 [60093], siAplp1-1 [159681], siAplp1-2 [159682], siAplp2-1 [160719], siAplp2-2 [160720]. Non-silencing siRNA duplexes were used as negative control (Qiagen).

2.3. Transfection of siRNA duplexes

The day before transfection, cells were trypsinized, diluted with fresh medium lacking antibiotics, and seeded into 24-well culture plates (1×10^4 cells/well). Transfection of siRNA duplexes was carried out using jetSI (Polyplus transfection) according to the manufacturer's instructions, with minor modifications. Before transfection, the culture medium was replaced with 0.4 ml OPTI-MEM I (Invitrogen), and to each well, 40 nM siRNA duplex was applied. Cells were incubated for 4 h at 37 °C. After the 4 h incubation, 1 ml of the fresh culture medium without antibiotics was added, and further incubation was carried out.

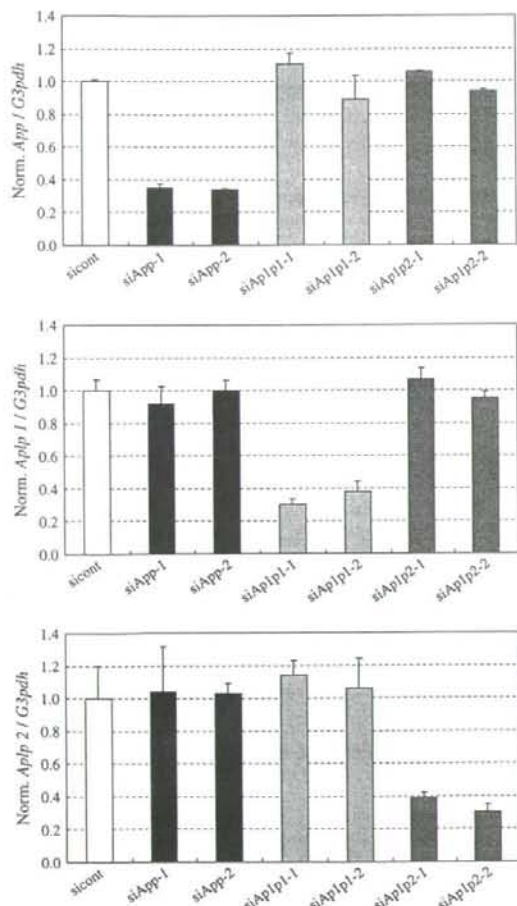


Fig. 1. Expression profiles of *App*, *Aplp1* and *Aplp2* in N2a cells. Indicated siRNA duplexes were transfected into N2a cells. Twelve hours after transfection, total RNA was extracted from the cells, and was subjected to RT-(real-time) PCR. Expression levels of *App*, *Aplp1*, or *Aplp2* were normalized against those of *G3pdh*, and the ratios of expression levels were normalized against the ratio obtained in the presence of the siControl duplex. Data are means of at least three independent determinations. Error bars represent standard deviations.

2.4. Reverse transcription-(real-time) polymerase chain reaction

In order to examine the expression levels of the genes, total RNA was extracted from cells and was subjected to reverse transcription-(real-time) polymerase chain reaction [RT-(real-time) PCR], as described previously (Hohjoh, 2004; Ohnishi et al., 2006; Sago et al., 2004). Real-time PCR was carried out using the ABI PRISM 7300 sequence detection system (Applied Biosystems) with a TaqMan Universal PCR Master Mix together with Assays-on-Demand Gene Expression products (Applied Biosystems) according to the manufacturer's instructions. The Assays-on-Demand Gene Expression products used (Assay ID number) were as follows: *App*; Mm00431827_m1, *Aplp1*; Mm00545893_m1, *Aplp2*; Mm00507819_m1.

2.5. Western blotting

Cell lysate and culture media were examined by Western blotting as described previously (Ohnishi et al., 2006). Equal amounts of proteins were separated by SDS-PAGE and electrophoretically blotted onto PVDF membranes (Millipore). Membranes were blocked with 5% non-fat milk in PBS containing 0.05% Tween-20 and incubated with anti-APP mouse monoclonal (3E9) antibody (MBL), anti-APLP1 rabbit polyclonal antibody (Calbiochem) and anti- α -tubulin (Sigma) antibody followed by washing in PBS and further incubation with horseradish peroxidase-conjugated anti-mouse IgG (Jackson ImmunoResearch Labs) or biotinylated anti-rabbit IgG together with avidin-biotinylated horseradish peroxidase complexes (Vectastain). Antigen-antibody complexes were visualized using ECL chemiluminescent reagent (Amersham).

2.6. Cell viability assay

Cell viability was investigated using 3-(4,5-dimethylthiazol-2-yl)-5-(3-carboxymethoxyphenyl)-2-(4-sulfophenyl)-2H-tetrazolium (MTS) assay using a CellTiter 96 aqueous non-radioactive cell proliferation assay kit (Promega) according to the manufacturer's instructions.

3. Results and discussion

Because the *App*, *Aplp1* and *Aplp2* genes are members of the same gene family, we first assessed whether sequence-specific

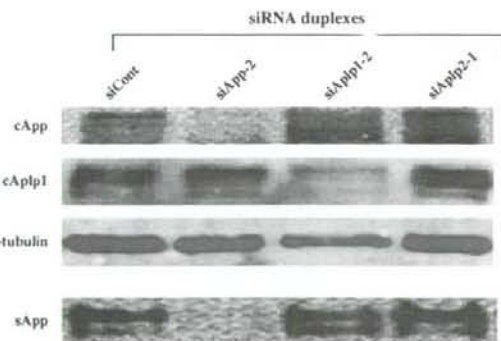


Fig. 2. Western blot analysis of *App* and *Aplp1*. Transfection of indicated siRNA duplexes into N2a cells was carried out as described for Fig. 1. Twenty-four hours after transfection, culture medium was replaced with DMEM without serum, and further 24 h culture was carried out. Cell lysate and culture media were prepared from transfected cells, and expressed *App* and *Aplp1* in cells (cellular *App* and *Aplp1*: cApp and cAplp1) and *App* in culture media (secreted *App*: sApp) were examined by Western blotting. Expression of α -tubulin (control) was also examined. As for *Aplp2*, we could not obtain antibody against it in this study.

gene silencing (RNAi) was induced by siRNA duplexes. Twelve hours after transfection with the siRNA duplexes targeting *App*, *Aplp1* and *Aplp2*, the expression levels of the target genes were examined by means of RT-(real-time) PCR

and Western blotting. As shown in Figs. 1 and 2, the results indicate that used siRNA duplexes were able to inhibit the expression of their own target genes without suppressing the expression of the other two genes, thus suggesting that specific

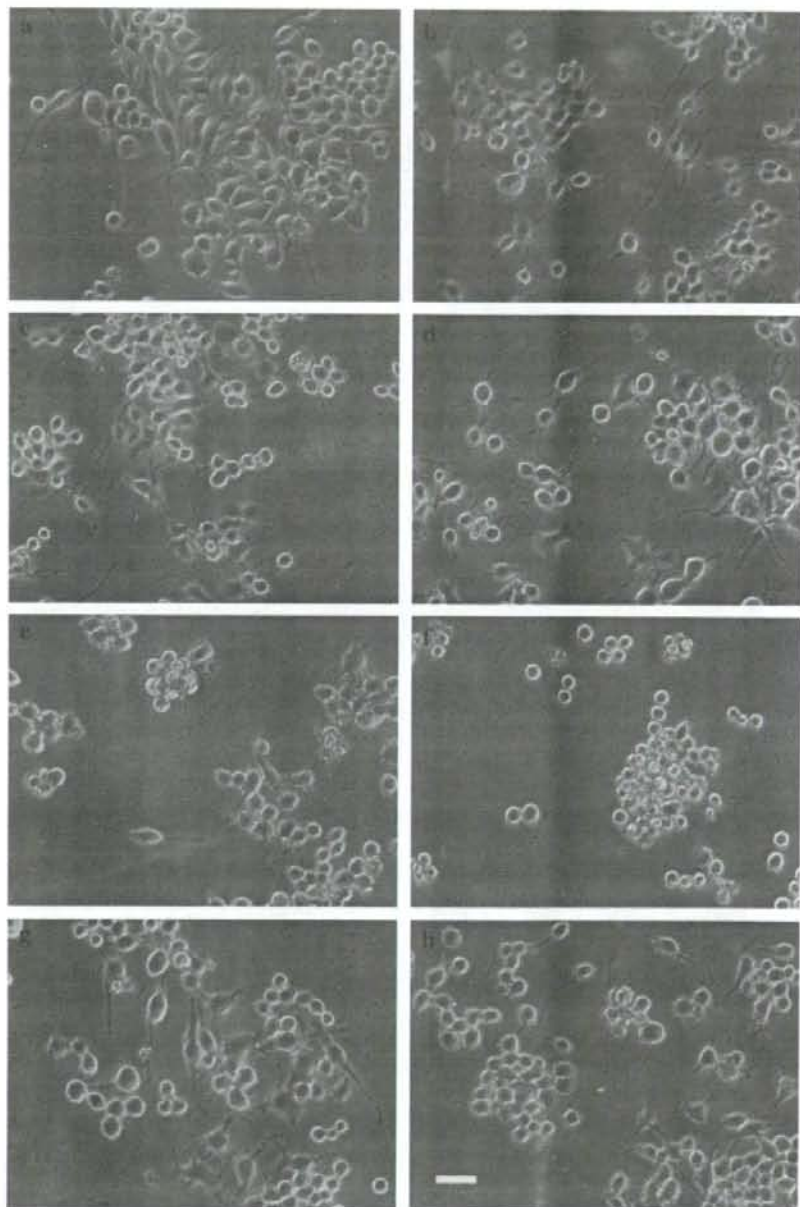


Fig. 3. Morphological differentiation of N2a cells with knockdown of *App*, *Aplp1* and *Aplp2*. Transfection of siRNA duplexes into N2a cells was carried out as described for Fig. 1. Twenty-four hours after transfection, culture medium was replaced with DMEM without serum, and further 24 h culture was carried out as described for Fig. 2. Transfected siRNA duplexes were as follows: (a) no siRNA (jetSI reagent alone); (b) siControl; (c) siApp-1; (d) siApp-2; (e) siAplp1-1; (f) siAplp1-2; (g) siAplp2-1; (h) siAplp2-2. Scale bar indicates 50 μ m.

inhibition of target gene expression was induced by the siRNA duplexes.

Because N2a cells are differentiated by serum deprivation [the resultant cells exhibit differentiated morphology with long neuritic processes (Fig. 3a)] (Diaz-Nido et al., 1988), we investigated the morphological differentiation of N2a cells with knockdown of *App*, *Aplp1* and *Aplp2* under serum deprivation. Fig. 3 shows photographs of N2a cells treated with siRNA duplexes after 24 h culture in the absence of serum. Neurite outgrowth was examined based on cell body diameter (approximately 15 μ m) and cells with extended neurites longer than two cell body diameters were judged to be differentiated. As shown in the figure, moderate levels of neurite outgrowth were observed in N2a cells undergoing gene silencing of *App* and *Aplp2*; in contrast, very little neurite outgrowth was seen in N2a cells with knockdown of *Aplp1*. In addition, based on the observation of transfected cells, it appears that knockdown of the *App* gene family also influences cell viability. To further confirm this observation, we examined cell viability by means of MTS assay. As shown in Fig. 4, the results indicate that: (i) N2a cells with knockdown of *Aplp1* exhibit significantly reduced viability under the present culture conditions, in both the presence and absence of serum; (ii) knockdown of *App* apparently decreases cell viability under serum deprivation, but does not significantly affect viability in the presence of serum; and (iii) knockdown of *Aplp2* in N2a cells has little influence on cell viability. Taken together with the results of Fig. 3, it is possible that the inhibition of neurite outgrowth may be associated with decreased cell viability in N2a cells with knockdown of *Aplp1*.

Previous studies of *App*, *Aplp1* and *Aplp2* knockout mice have suggested that *App* family members possess essential, but partially

redundant, functions, and that they play important roles in normal brain development and early postnatal survival (Heber et al., 2000; Herms et al., 2004; von Koch et al., 1997). Of the *App* family members, *Aplp2* may have a key function, as *Aplp2*^{-/-}*App*^{-/-} and *Aplp2*^{-/-}*Aplp1*^{-/-} double knockout mice are postnatally lethal, while *App*^{-/-}*Aplp1*^{-/-} double knockout mice are viable. However, *Aplp2*^{-/-} single knockout mice appeared to be normal (von Koch et al., 1997), whereas *Aplp1*^{-/-} single knockout mice exhibited postnatal growth deficit (Heber et al., 2000).

Based on the present observations, *Aplp1* rather than *Aplp2* appears to play an important role in Neuro2a cells. Because *Aplp1* is specifically expressed in the nervous system (Lorent et al., 1995), it is possible that *Aplp1* plays an essential role in the survival and differentiation of neuronal cells (at least N2a cells). The present and previous observations also suggest that different cells (tissues) may require different contributions by the *App* gene family. To further evaluate these possibilities, more extensive studies are required.

Acknowledgments

We would like to thank Y. Ohnishi and Y. Tamura for their helpful assistance. This work was supported in part by research grants from the Ministry of Health, Labor and Welfare of Japan.

References

- Diaz-Nido J, Serrano L, Mendez E, Avila J. A casein kinase II-related activity is involved in phosphorylation of microtubule-associated protein MAP-1B during neuroblastoma cell differentiation. *J Cell Biol* 1988;106:2057–65.
- Eggert S, Paliga K, Soba P, Evlin G, Masters CL, Weidemann A, et al. The proteolytic processing of the amyloid precursor protein gene family members APLP-1 and APLP-2 involves alpha-, beta-, gamma-, and epsilon-like cleavages: modulation of APLP-1 processing by *n*-glycosylation. *J Biol Chem* 2004;279:18146–56.
- Gu Y, Misonou H, Sato T, Dohmae N, Takio K, Ihara Y. Distinct intramembrane cleavage of the beta-amyloid precursor protein family resembling gamma-secretase-like cleavage of Notch. *J Biol Chem* 2001;276:35235–8.
- Heber S, Herms J, Gajic V, Hainfellner J, Aguzzi A, Rulicke T, et al. Mice with combined gene knock-outs reveal essential and partially redundant functions of amyloid precursor protein family members. *J Neurosci* 2000; 20:7951–63.
- Herms J, Anliker B, Heber S, Ring S, Fuhrmann M, Kretschmar H, et al. Cortical dysplasia resembling human type 2 lissencephaly in mice lacking all three APP family members. *EMBO J* 2004;23:4106–15.
- Hohjoh H. Enhancement of RNAi activity by improved siRNA duplexes. *FEBS Lett* 2004;557:193–8.
- Li Q, Sudhof TC. Cleavage of amyloid-beta precursor protein and amyloid-beta precursor-like protein by BACE 1. *J Biol Chem* 2004;279:10542–50.
- Lorent K, Overbergh L, Moechars D, De Strooper B, Van Leuven F, Van den Berghe H. Expression in mouse embryos and in adult mouse brain of three members of the amyloid precursor protein family, of the alpha-2-macroglobulin receptor/low density lipoprotein receptor-related protein and of its ligands apolipoprotein E, lipoprotein lipase, alpha-2-macroglobulin and the 40,000 molecular weight receptor-associated protein. *Neuroscience* 1995;65:1009–25.
- Ohnishi Y, Tokunaga K, Kaneko K, Hohjoh H. Assessment of allele-specific gene silencing by RNA interference with mutant and wild-type reporter alleles. *J RNAi Gene Silencing* 2006;2:154–60.
- Sago N, Omi K, Tamura Y, Kunugi H, Toyo-oka T, Tokunaga K, et al. RNAi induction and activation in mammalian muscle cells where Dicer and

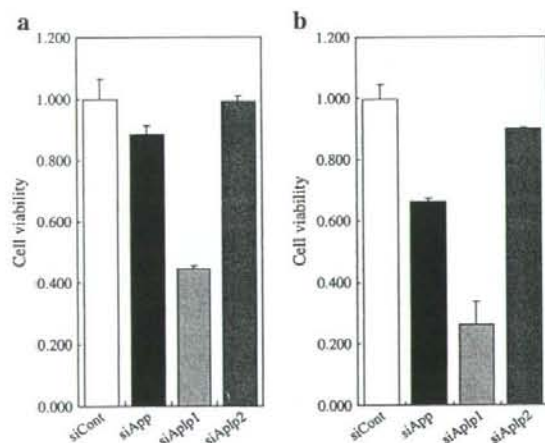


Fig. 4. Cell viability of N2a cells undergoing gene silencing of *App*, *Aplp1* and *Aplp2*. Transfection of siRNA duplexes was carried out as described for Fig. 1. Twenty-four hours after transfection, culture medium was replaced with DMEM with (A) or without (B) 10% serum. Seventy-two hours after transfection, cell viability was examined by means of MTS assay. Cell viability in the presence of siRNA duplexes against *App*, *Aplp1*, and *Aplp2* was normalized against that in the presence of siControl. Data are means of three independent experiments. Error bars represent standard deviations.

- eIF2C translation initiation factors are barely expressed. *Biochem Biophys Res Commun* 2004;319:50–7.
- Scheinfeld MH, Ghersi E, Laky K, Fowlkes BJ, D'Adamio L. Processing of beta-amyloid precursor-like protein-1 and -2 by gamma-secretase regulates transcription. *J Biol Chem* 2002;277:44195–201.
- Slunt HH, Thinakaran G, Von Koch C, Lo AC, Tanzi RE, Sisodia SS. Expression of a ubiquitous, cross-reactive homologue of the mouse beta-amyloid precursor protein (APP). *J Biol Chem* 1994;269:2637–44.
- Turner PR, O'Connor K, Tate WP, Abraham WC. Roles of amyloid precursor protein and its fragments in regulating neural activity, plasticity and memory. *Prog Neurobiol* 2003;70:1–32.
- von Koch CS, Zheng H, Chen H, Trumbauer M, Thinakaran G, van der Plöeg LH, et al. Generation of APLP2 KO mice and early postnatal lethality in APLP2/APP double KO mice. *Neurobiol Aging* 1997;18:661–9.
- Wasco W, Bupp K, Magendantz M, Gusella JF, Tanzi RE, Solomon F. Identification of a mouse brain cDNA that encodes a protein related to the Alzheimer disease-associated amyloid beta protein precursor. *Proc Natl Acad Sci U S A* 1992;89:10758–62.
- Wasco W, Brook JD, Tanzi RE. The amyloid precursor-like protein (APLP) gene maps to the long arm of human chromosome 19. *Genomics* 1993a;15:237–9.
- Wasco W, Gurubhagavatula S, Paradis MD, Romano DM, Sisodia SS, Hyman BT, et al. Isolation and characterization of APLP2 encoding a homologue of the Alzheimer's associated amyloid beta protein precursor. *Nat Genet* 1993b;5:95–100.

Degradation of Amyotrophic Lateral Sclerosis-linked Mutant Cu,Zn-Superoxide Dismutase Proteins by Macroautophagy and the Proteasome^{*[5]}

Received for publication, April 7, 2006, and in revised form, August 18, 2006. Published, JBC Papers in Press, August 18, 2006, DOI 10.1074/jbc.M603337200

Tomohiro Kabuta, Yasuyuki Suzuki, and Keiji Wada¹

From the Department of Degenerative Neurological Diseases, National Institute of Neuroscience, National Center of Neurology and Psychiatry, Kodaira, Tokyo 187-8502, Japan

Mutations in the Cu,Zn-superoxide dismutase (SOD1) gene cause ~20% of familial cases of amyotrophic lateral sclerosis (fALS). Accumulating evidence indicates that a gain of toxic function of mutant SOD1 proteins is the cause of the disease. It has also been shown that the ubiquitin-proteasome pathway plays a role in the clearance and toxicity of mutant SOD1. In this study, we investigated the degradation pathways of wild-type and mutant SOD1 in neuronal and nonneuronal cells. We provide here the first evidence that wild-type and mutant SOD1 are degraded by macroautophagy as well as by the proteasome. Based on experiments with inhibitors of these degradation pathways, the contribution of macroautophagy to mutant SOD1 clearance is comparable with that of the proteasome pathway. Using assays that measure cell viability and cell death, we observed that under conditions where expression of mutant SOD1 alone does not induce toxicity, macroautophagy inhibition induced mutant SOD1-mediated cell death, indicating that macroautophagy reduces the toxicity of mutant SOD1 proteins. We therefore propose that both macroautophagy and the proteasome are important for the reduction of mutant SOD1-mediated neurotoxicity in fALS. Inhibition of macroautophagy also increased SOD1 levels in detergent-soluble and -insoluble fractions, suggesting that both detergent-soluble and -insoluble SOD1 are degraded by macroautophagy. These findings may provide further insights into the mechanisms of pathogenesis of fALS.

Amyotrophic lateral sclerosis (ALS)² is a neurodegenerative disease caused by selective loss of motor neurons (1, 2).

^{*} This work was supported by grants-in-aid for scientific research from the Japan Society for the Promotion of Science; a research grant in a priority area of research from the Ministry of Education, Culture, Sports, Science, and Technology, Japan; grants-in-aid for scientific research from the Ministry of Health, Labor and Welfare, Japan; and the Program for Promotion of Fundamental Studies in Health Sciences of the National Institute of Biomedical Innovation, Japan. The costs of publication of this article were defrayed in part by the payment of page charges. This article must therefore be hereby marked "advertisement" in accordance with 18 U.S.C. Section 1734 solely to indicate this fact.

^[5] The on-line version of this article (available at <http://www.jbc.org>) contains supplemental Figs. 51–56.

¹ To whom correspondence should be addressed: Dept. of Degenerative Neurological Diseases, National Institute of Neuroscience, National Center of Neurology and Psychiatry, 4-1-1 Ogawahigashi, Kodaira, Tokyo 187-8502, Japan. Tel: 81-42-346-1715; Fax: 81-42-346-1745; E-mail: wada@ncnp.go.jp.

² The abbreviations used are: ALS, amyotrophic lateral sclerosis; fALS, familial ALS; SOD1, Cu,Zn-superoxide dismutase(s); 3-MA, 3-methyladenine; siRNA, short interfering RNA; EGFP, enhanced green fluorescent protein; HA, hemag-

glutinin; MTS, 3-(4,5-dimethylthiazol-2-yl)-5-(3-carboxymethoxyphenyl)-2-(4-sulfophenyl)-2H-tetrazolium.

Although most cases of ALS are sporadic, ~10% of ALS cases run in families. Dominant missense mutations in the gene that encodes the Cu,Zn-superoxide dismutase (SOD1) are responsible for 20% of familial ALS (fALS) cases (3). Mice overexpressing mutant SOD1 develop an ALS-like phenotype comparable with human ALS, whereas mice lacking SOD1 do not (4, 5). These findings have led to the conclusion that SOD1 mutants cause motor neuron degeneration by a toxic gain of function. Thus, studies of the degradation process of mutant SOD1 proteins could provide important insights into understanding the mechanisms that underlie the pathology of fALS, and possibly sporadic ALS, and into developing novel therapies for fALS by removing toxic species of mutant SOD1.

Cytoplasmic proteins are mainly degraded by two pathways, the ubiquitin-26 S proteasome pathway (6) and autophagy (7). Previous studies have shown that mutant SOD1 proteins are turned over more rapidly than wild-type SOD1, and a proteasome inhibitor increases the level of mutant SOD1 proteins (8, 9). Dornif and NEDL1, two distinct ubiquitin ligases, ubiquitinate mutant but not wild-type SOD1 (10, 11). These observations suggest that mutant SOD1 is degraded by the ubiquitin-26 S proteasome pathway and that the increased turnover of mutant SOD1 is mediated in part by this pathway. On the other hand, the 20 S proteasome, a component of the 26 S proteasome, can degrade proteins without a requirement for ubiquitination (12, 13). A recent study has found that metal-free forms of wild-type and mutant SOD1 are degraded by the 20 S proteasome *in vitro* (14).

Autophagy is an intracellular process that results in the degradation of cytoplasmic components inside lysosomes. At least three forms of autophagy have been described in mammalian cells: macroautophagy, microautophagy, and chaperone-mediated autophagy (7). Macroautophagy is the major and the most well studied form of autophagy; this process begins with a sequestration step, in which cytosolic components are engulfed by a membrane sac called the isolation membrane. This membrane results in a double membrane structure called the autophagosome, which fuses with the lysosome. The inner membrane of the autophagosome and its protein and organelle contents are degraded by lysosomal hydrolases. Recent reports have demonstrated that macroautophagy plays an important role in preventing neurodegeneration in mice (15, 16). Although macroautophagy can be induced by starvation, this

glutinin; MTS, 3-(4,5-dimethylthiazol-2-yl)-5-(3-carboxymethoxyphenyl)-2-(4-sulfophenyl)-2H-tetrazolium.

pathway may take place constitutively in mammals (17). In cultured cells, inhibition of macroautophagy does not alter enhanced green fluorescent protein (EGFP) levels (18) or glyceraldehyde-3-phosphate dehydrogenase protein levels,³ suggesting that not all cytosolic proteins are degraded by macroautophagy. To date, however, there have been no reports of macroautophagy in mutant SOD1 clearance.

In this study, we investigated the pathway by which human wild-type SOD1 and the A4V, G85R, and G93A SOD1 mutants are degraded in neuronal and nonneuronal cells. We show that wild-type and mutant SOD1 proteins are degraded by both the proteasomal pathway and macroautophagy. The experiments with inhibitors of these degradation pathways suggested that mutant SOD1 are degraded more rapidly than wild-type SOD1 in part by macroautophagy and that the contribution of macroautophagy to mutant SOD1 clearance is approximately equal to that of the proteasome pathway. Macroautophagy decreases mutant SOD1 protein levels in both nonionic detergent-soluble and -insoluble fractions. In addition, we provide data indicating that macroautophagy has a role in mutant SOD1-mediated cell death.

EXPERIMENTAL PROCEDURES

Plasmid Constructs—The expression plasmids pDNA3-hSOD1 containing wild-type, A4V, G85R, and G93A mutant SOD1 were kindly donated by Ryosuke Takahashi (Kyoto University, Kyoto, Japan) and Makoto Urushitani (Laval University, Quebec, Canada) (19). To construct a plasmid expressing human wild-type SOD1 with the HA tag at the carboxyl terminus of SOD1, HA-tagged SOD1 fragments were amplified by PCR using wild-type SOD1 cDNA (Open Biosystems, Huntsville, AL) as the template. The PCR products were digested with XhoI and NotI and cloned into an XhoI-NotI-digested pCI-neo vector (Promega, Madison, WI). The primers used were 5'-AAAACCTCGAGCCGCAAGATGGCGACGAAGGCCGTGTGCG-3' and 5'-AAAAGCGCCGCTTAAGCGTAATCTGGAACATCGTATGGGTATTGGGCGATCCCAATTACACCACA-3'. A plasmid expressing HA-tagged G93A SOD1 was generated using QuikChange site-directed mutagenesis kit (Stratagene, La Jolla, CA) according to the manufacturer's protocol. To construct a plasmid expressing fusion protein of green fluorescent protein and LC3, LC3 fragments were amplified by PCR using rat LC3 cDNA (Open Biosystems) as the template. The PCR products were digested with BglII and EcoRI and cloned into a BglII-EcoRI-digested pEGFP-C1 vector (Clontech). The primers used were 5'-ACTCAGATCTATGCCGTCCGAGAAGACCTCAAAA-3' and 5'-TGCAGAATTCTTACACAGCCAGTGTGTCCCGAA-3'. After construction, the DNA sequences of the plasmids were confirmed by DNA sequence analysis.

Cell Culture and Transfection—The mouse neuroblastoma cell line Neuro2a, the human neuroblastoma cell line SH-SY5Y, and the monkey kidney-derived cell line COS-7 were maintained in Dulbecco's modified Eagle's medium (Sigma) supplemented with 10% fetal calf serum (JRH Biosciences, Lenexa, KS). Transient expression of each vector in Neuro2a and COS-7 cells was performed using the FuGENE 6 transfection reagent

(Roche Applied Science). For experiments with differentiated Neuro2a cells, the medium was changed to differentiation medium (Dulbecco's modified Eagle's medium supplemented with 1% fetal calf serum and 20 μ M retinoic acid) 24 h after transfection. Approximately 90% of cells in dishes (wells) were transfected in our experimental conditions (data not shown), and there was no notable differences in the transfection efficiency among the wells (supplemental Fig. S1).

Treatment of Cells with Epoxomicin, 3-Methyladenine, Cycloheximide, Rapamycin, or NH₄Cl—Cells grown in 12- or 6-well plates to 50–80% confluence were transfected with expression plasmids containing wild-type, A4V, G85R, or G93A mutant SOD1. 24 h after transfection, cells were incubated with epoxomicin (10 nM, 1 μ M, 5 μ M, or 10 μ M; Sigma), 3-methyladenine (3-MA) (10, 20, or 30 mM; Sigma), rapamycin (100 or 200 nM; Sigma), 20 mM NH₄Cl, and/or carrier (Me₂SO or water) as a control. In some experiments, 10 μ g/ml cycloheximide (Sigma) was added to the cells to avoid the confounding effects of ongoing protein synthesis. Epoxomicin, cycloheximide, and rapamycin were dissolved in Me₂SO, NH₄Cl in water. 3-MA was freshly dissolved in culture medium 30 min before use.

Cell Fractionation—For preparation of nonionic detergent-soluble and -insoluble fractions, adherent cells were harvested and lysed on ice for 15 min in 1% Triton X-100 lysis buffer containing 50 mM Tris-HCl, pH 7.5, 150 mM NaCl, 5 mM EDTA, 1% Triton X-100, and protease inhibitors (Complete, EDTA-free; Roche Applied Science). Lysates were centrifuged at 20,000 \times g for 10 min at 4 °C, and the supernatants were pooled and designated as the detergent-soluble fractions. After the pellets were washed with 1% Triton X-100 lysis buffer, they were solubilized with SDS buffer (50 mM Tris-HCl, pH 7.5, 150 mM NaCl, 5 mM EDTA, 3% SDS, 1% Triton X-100, and protease inhibitors) and sonicated. The resulting solution was used as the detergent-insoluble fraction. For preparation of total cell lysates containing both detergent-soluble and -insoluble fractions, cells were lysed in SDS buffer and sonicated. Protein concentrations were determined with the protein assay kit (Bio-Rad) or the DC protein assay kit (Bio-Rad).

Western Blot Analysis—Western blotting was performed using standard procedures as described previously (20). The primary antibodies used were as follows: anti-SOD1 rabbit polyclonal antibody (1:4000; Stressgen Bioreagents, Victoria, Canada), anti- α -tubulin mouse monoclonal antibody (1:4000; Sigma), anti- β -actin mouse monoclonal antibody (1:5000; Sigma), anti-HA mouse monoclonal antibody (1:4000; Sigma), anti-Becn1 mouse monoclonal antibody (1:500; BD Transduction Laboratories, San Diego, CA), anti-Apg7/Atg7 rabbit polyclonal antibody (1:500; Rockland, Gilbertsville, PA). After overnight incubation with primary antibodies at 4 °C, each blot was probed with horseradish peroxidase-conjugated anti-rabbit IgG or anti-mouse IgG (1:20,000; Pierce). Immunoreactive signals were visualized with SuperSignal West Dura extended duration substrate (Pierce) or SuperSignal West Femto maximum sensitivity substrate (Pierce) and detected with a chemiluminescence imaging system (FluorChem; Alpha Innotech, San Leandro, CA). The signal intensity was quantified by densitometry using FluorChem software (Alpha Innotech).

Short Interfering RNA (siRNA) Preparation and Transfection—Double-stranded siRNA targeting mouse Becn1, mouse Atg7 and EGFP were purchased from RNAi Co., Ltd.

³ T. Kabuta, Y. Suzuki, and K. Wada, unpublished data.

Degradation of Mutant SOD1 by Macroautophagy

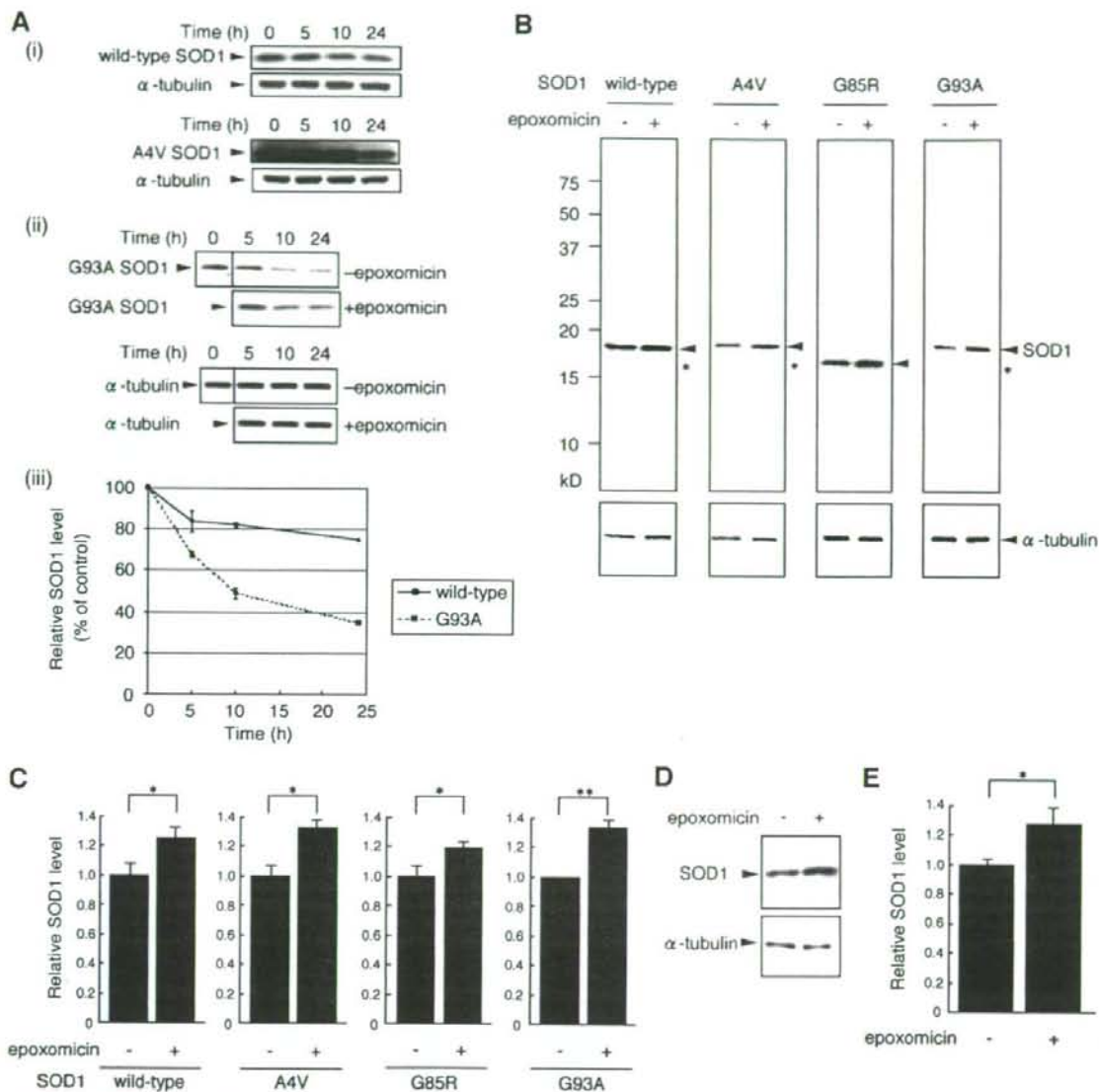


FIGURE 1. Both mutant and wild-type SOD1 are degraded by the proteasome. *A, i*, Neuro2a cells were transiently transfected with wild-type or mutant A4V human SOD1. 24 h after transfection, cells were treated with 10 μ g/ml cycloheximide for the indicated time and lysed. Total cell lysates were analyzed by immunoblotting using anti-SOD1 or anti- α -tubulin antibody. *ii*, Neuro2a cells transfected with G93A SOD1 were incubated with or without 10 nM epoxomicin in the presence of 10 μ g/ml cycloheximide for the indicated time and lysed. Total cell lysates were analyzed by immunoblotting using anti-SOD1 or anti- α -tubulin antibody. *iii*, the relative levels of wild-type or G93A SOD1 (percentage of 0-h control) were quantified by densitometry. Mean values are shown with S.E. ($n = 3$). *B* and *C*, Neuro2a cells were transiently transfected with wild-type or mutant A4V, G85R, or G93A human SOD1. 24 h after transfection, cells were incubated with or without 10 nM epoxomicin in the presence of 10 μ g/ml cycloheximide for 24 h. Total cell lysates were analyzed by immunoblotting using anti-SOD1 antibody. The electrophoretic mobility of G85R SOD1 was greater than that of wild-type SOD1. α -Tubulin was used as a loading control. Asterisks indicate endogenous mouse SOD1 (*B*). The relative level of wild-type or mutant SOD1 was quantified by densitometry. Mean values are shown with S.E. ($n = 3$). *, $p < 0.05$; **, $p < 0.01$ (*C*). *D* and *E*, human SH-SY5Y cells were incubated with or without 10 nM epoxomicin in the presence of cycloheximide for 24 h. Total cell lysates were analyzed by immunoblotting with anti-SOD1 antibody (*D*). The relative level of human endogenous SOD1 was quantified by densitometry. Data are expressed as the means \pm S.E. ($n = 3$). *, $p < 0.05$ (*E*).

(Tokyo, Japan). Sequences targeted by siRNA were selected using siDirect (RNAi Co., Ltd.): mouse Beclin 1 siRNA, sense (5'-GUC-UACAGAAAGUGCUAAUAG-3') and antisense (5'-AUUAGC-ACUUCUCUGUAGACAU-3'); mouse Atg7 siRNA, sense (5'-GAGCGGCGGCUUGUAGAACA-3') and antisense (5'-UUC-

UUACCAGCCGCCGCUCA-3'); EGFP siRNA, sense (5'-GCC-ACAACGUCUAUAUCAUGG-3') and antisense (5'-AUGAUA-UAGACGUUGUGGCUG-3'). EGFP siRNA was used as a control. Cells (3×10^6) were cotransfected with 1 μ g of DNA and 3 μ g of siRNA using Lipofectamine PLUS reagent (Invitrogen).

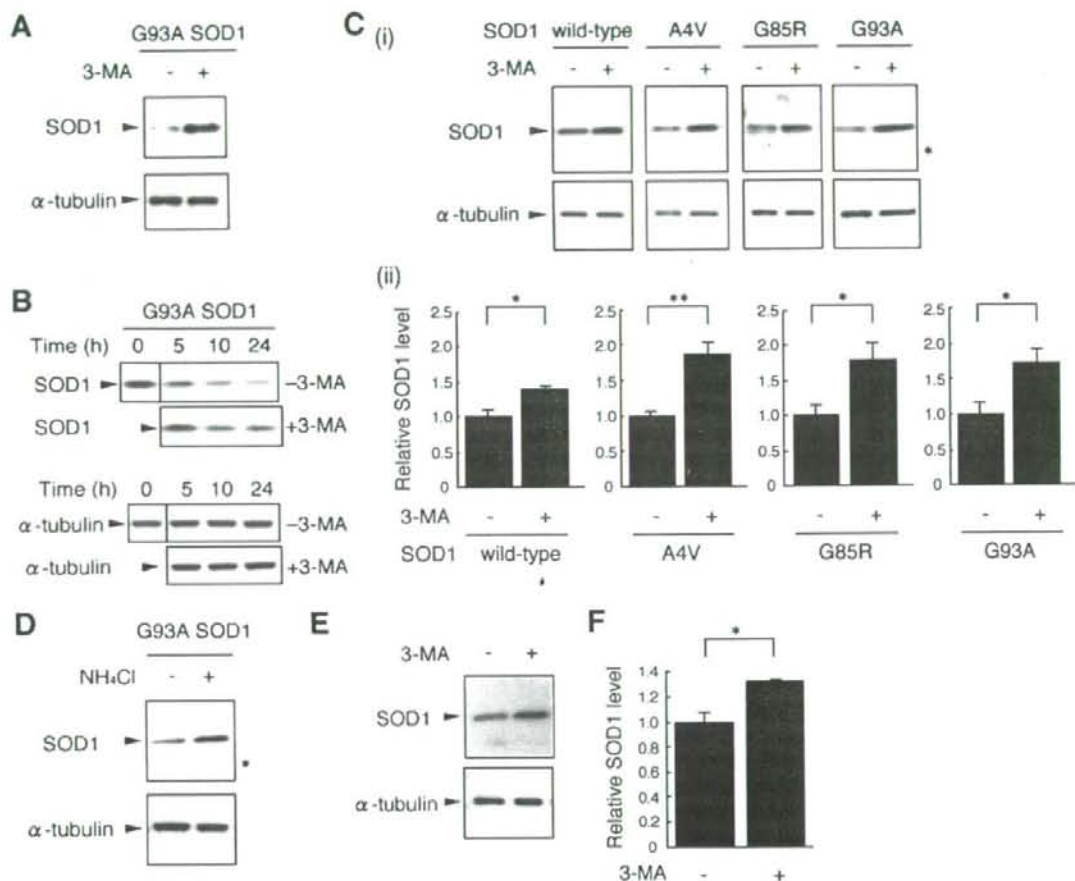


FIGURE 2. Wild-type and mutant SOD1 are degraded by macroautophagy. *A*, Neuro2a cells were transiently transfected with the G93A mutant SOD1. 24 h after transfection, cells were incubated with or without 10 mM 3-MA for 24 h. Total cell lysates were analyzed by immunoblotting using anti-SOD1 antibody. α -Tubulin was used as a loading control. *B*, Neuro2a cells transfected with G93A SOD1 were incubated with or without 10 mM 3-MA in the presence of 10 μ M cycloheximide for the indicated time and lysed. Total cell lysates were analyzed by immunoblotting using anti-SOD1 or anti- α -tubulin antibody. *C*, Neuro2a cells transfected with wild-type or mutant A4V, G85R, or G93A SOD1 were incubated with or without 10 mM 3-MA in the presence of 10 μ M cycloheximide for 24 h. Total cell lysates were analyzed by immunoblotting. An asterisk indicates endogenous mouse SOD1 (*i*). The relative level of wild-type or mutant SOD1 was quantified by densitometry. Mean values are shown with S.E. ($n = 3$). *, $p < 0.05$; **, $p < 0.01$ (*ii*). *D*, Neuro2a cells transfected with G93A SOD1 were incubated with or without 20 mM NH_4Cl in the presence of cycloheximide for 24 h. Total cell lysates were analyzed by immunoblotting. An asterisk indicates endogenous mouse SOD1. *E* and *F*, SH-SY5Y cells were incubated with or without 10 mM 3-MA in the presence of cycloheximide for 24 h. Total cell lysates were analyzed by immunoblotting (*E*). The relative level of human endogenous SOD1 was quantified by densitometry. Data are expressed as the means \pm S.E. ($n = 3$). *, $p < 0.05$ (*F*).

Quantitative Assessment of Cell Viability and Cell Death—One day before transfection, Neuro2a cells were seeded at 5×10^5 cells/well in 24-well plates. 24 h after transfection with 0.4 μ g of DNA/well, cells were cultured in differentiation medium with or without 10 mM 3-MA for 24 h. Cell death was assessed by a lactate dehydrogenase release assay using the CytoTox-ONE homogeneous membrane integrity assay (Promega) according to the manufacturer's protocol. The percentage of cytotoxicity (Fig. 7G) was calculated according to this protocol. For assessment of cell viability, we used the 3-(4,5-dimethylthiazol-2-yl)-5-(3-carboxymethoxyphenyl)-2-(4-sulfophenyl)-2H-tetrazolium (MTS) assay and the ATP assay with the CellTiter 96 AQueous One Solution cell proliferation assay (Promega) and CellTiter-Glo luminescent cell viability assay (Promega), respectively, according to

the manufacturer's protocols. Measurements with a multiple-plate reader were performed after samples were transferred to 96-well assay plates.

Statistical Analysis—For comparison of two groups, the statistical difference was determined by Student's *t* test. For comparison of more than two groups, analysis of variance was used. If the analysis of variance was significant, Dunnett's multiple comparison test was used as a *post hoc* test.

RESULTS

Wild-type and Mutant SOD1 Are Degraded by the Proteasome—To determine whether SOD1 is degraded by the proteasome pathway, we assessed the effect of proteasome inhibitors on SOD1 protein clearance. Peptide aldehydes, such as

Degradation of Mutant SOD1 by Macroautophagy

MG132 or ALLN, and lactacystin are widely used proteasome inhibitors. However, peptide aldehydes also inhibit cathepsins and calpains, and lactacystin inhibits cathepsin A (21, 22). Because these inhibitors are not proteasome-specific and may interfere with lysosomal function, we used epoxomicin as a selective proteasome inhibitor (23, 24). We observed protein clearance of human SOD1 in Neuro2a cells transfected with mutant or wild-type SOD1 in the presence of the translation inhibitor cycloheximide (Fig. 1A, *i* and *ii*). Consistent with previous reports (9, 11), wild-type SOD1 exhibited a relatively long half-life (half-life of more than 24 h) compared with mutant SOD1 (~10 h; G93A) (Fig. 1A, *iii*). The degradation of wild-type and mutant SOD1 was suppressed by epoxomicin treatment (Fig. 1, B and C) (~14-h increase in half-life; G93A; Fig. 1A, *ii*). Our finding that mutant SOD1 is degraded by the proteasome is in agreement with previous reports (8, 9). To determine whether endogenous human wild-type SOD1 is also degraded by the proteasome, SOD1 clearance was examined using the human neuroblastoma SH-SY5Y cell line. The proteasome inhibitor treatment promoted the accumulation of human SOD1 proteins (Fig. 1, D and E). These results indicate that endogenous wild-type SOD1 is degraded by the proteasome, also consistent with a previous report (14).

Wild-type and Mutant SOD1 Are Also Degraded by Macroautophagy—To date, there have been no reports of macroautophagy participating in human SOD1 clearance. We therefore investigated whether wild-type or mutant SOD1 was degraded by macroautophagy using 3-MA, an inhibitor of macroautophagy (18, 25, 26), and ammonium chloride, an inhibitor of lysosomal proteolysis (26). We initially confirmed that 3-MA inhibits the formation of autophagosomes in Neuro2a cells using green fluorescent protein-LC3, a marker of autophagosomes (27) (supplemental Fig. S2). Moreover, we also showed that the clearance of α -synuclein, an established substrate for macroautophagy (28), was inhibited by 3-MA or ammonium chloride treatment (supplemental Fig. S3). Treatment of Neuro2a cells with 3-MA promoted the accumulation of G93A mutant SOD1 proteins (Fig. 2A). In the presence of cycloheximide, the degradation of wild-type and mutant SOD1 was suppressed by treatment with 3-MA (Fig. 2, B and C) (a more than 14-h increase in half-life; G93A, Fig. 2B), indicating that wild-type and mutant SOD1 are degraded by macroautophagy in these cells and that the accumulation of SOD1 proteins by 3-MA is not due to increased protein synthesis. These results, together with Fig. 1, suggest that mutant SOD1 are degraded more rapidly than wild-type SOD1 by macroautophagy (it is estimated that 15–20% of wild-type SOD1 and 25–30% of mutant SOD1 were degraded by macroautophagy during the 24-h incubation). The clearance of mutant G93A SOD1 was also decreased by treatment with ammonium chloride (Fig. 2D). As shown in Supplemental Fig. S4 and Fig. 2D, the protein level of endogenous mouse SOD1 was increased by 3-MA or ammonium chloride treatment. The result shown in Fig. 2D further supports the role of the lysosomes in SOD1 degradation. To test the role of macroautophagy on SOD1 degradation in differentiated neuronal cells or neurons, we also used differentiated Neuro2a cells. In differentiated Neuro2a cells, 3-MA increased both wild-type and mutant SOD1 protein levels in the presence or absence of



FIGURE 3. Rapamycin treatment decreases mutant SOD1 protein levels. A and B, Neuro2a cells were transiently transfected with HA-tagged G93A SOD1. 24 h after transfection, cells were incubated with or without 100 nM rapamycin for 24 h. Total cell lysates were analyzed by immunoblotting using anti-SOD1 antibody. α -Tubulin was used as a loading control (A). The relative level of mutant G93A SOD1 was quantified by densitometry. Data are presented as the means \pm S.E. ($n = 3$). $*p < 0.05$ (B). C, Neuro2a cells transfected with mutant A4V, G85R, or G93A SOD1 were cultured in differentiation medium with or without 200 nM rapamycin for 24 h. Total cell lysates were analyzed by immunoblotting.

cycloheximide (data not shown). To determine whether endogenous human SOD1 is degraded by macroautophagy, the clearance of endogenous SOD1 was examined in SH-SY5Y cells. As shown in Fig. 2, E and F, the degradation of endogenous SOD1 proteins was inhibited by 3-MA.

For further confirmation of the clearance of SOD1 by macroautophagy, we used rapamycin to induce macroautophagy (29, 30), and gene silencing with siRNA to inhibit macroautophagy. Treating Neuro2a cells with rapamycin decreased HA-tagged G93A SOD1 levels (Fig. 3, A and B). In differentiated Neuro2a cells, SOD1 protein levels were also decreased by rapamycin (Fig. 3C). Beclin 1 is a component of a class III phosphatidylinositol 3-kinase complex that is crucial for macroautophagy (31). Silencing of the Beclin 1 gene by siRNA inhibits the generation of autophagosomes, thus preventing macroautophagy (32). Atg7 protein is also essential for macroautophagy (17). We initially confirmed that Beclin 1 or Atg7 expression was knocked down by Beclin 1 or Atg7 siRNA, respectively (Fig. 4, A and B). We also showed that α -synuclein level was increased by Beclin 1 or Atg7 siRNA (supplemental Fig. S3). We observed inhibited degradation of wild-type and mutant SOD1 in cells with Beclin 1 siRNA (Fig. 4, A and C) or Atg7 siRNA (Fig. 4, B and D) compared with cells with control siRNA (~14 h increase in half-life; G93A; Fig. 4E). The results shown in Figs. 2–4 demonstrate that wild-type and mutant SOD1 are also

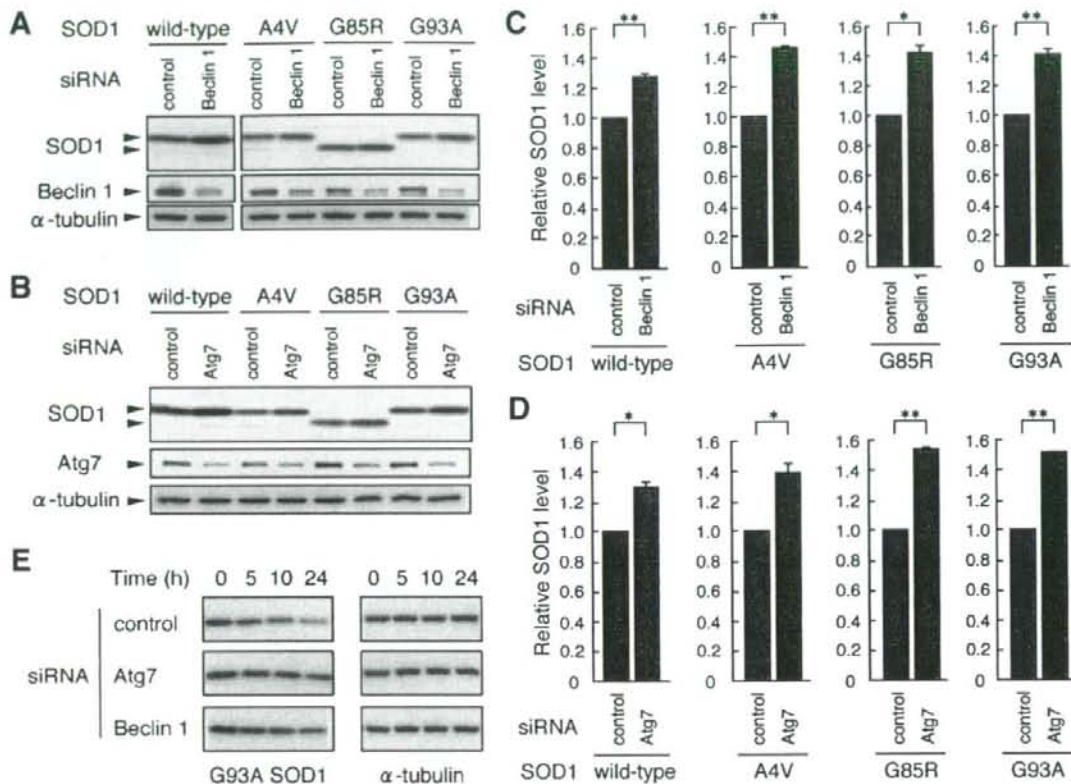


FIGURE 4. Silencing of macroautophagy genes promote the accumulation of SOD1 proteins. *A* and *C*, Neuro2a cells were cotransfected with SOD1 (wild-type, A4V, G85R, or G93A) and siRNA (Beclin 1 siRNA or control EGFP siRNA). 24 h after transfection, total cell lysates were prepared and analyzed by immunoblotting using anti-SOD1 or anti-Beclin 1 antibody. α -Tubulin was used as a control (*A*). Levels of SOD1 were quantified by densitometry, and the levels are expressed as -fold level of SOD1 in cells with Beclin 1 siRNA over cells with control siRNA. Data are presented as the means \pm S.E. ($n = 3$). $^* p < 0.05$; $^{**} p < 0.01$ (*C*). *B* and *D*, Neuro2a cells were cotransfected with SOD1 (wild-type, A4V, G85R, or G93A) and siRNA (Atg7 siRNA or control siRNA). 24 h after transfection, total cell lysates were prepared and analyzed by immunoblotting using anti-SOD1, anti-Atg7, or anti- α -tubulin antibody (*B*). Levels of SOD1 were quantified by densitometry, and the levels are expressed as -fold level of SOD1 in cells with Atg7 siRNA over cells with control siRNA. Data are presented as the means \pm S.E. ($n = 3$). $^* p < 0.05$; $^{**} p < 0.01$ (*D*). *E*, Neuro2a cells cotransfected with G93A SOD1 and siRNA (control, Atg7, or Beclin 1 siRNA) were treated with $10 \mu\text{g/ml}$ cycloheximide for the indicated time and lysed. Total cell lysates were analyzed by immunoblotting using anti-SOD1 or anti- α -tubulin antibody.

degraded by macroautophagy in neuronal cells. In the nonneuronal COS-7 cells, ammonium chloride or 3-MA treatment stimulated the accumulation of HA-tagged wild-type SOD1 and G93A SOD1 (Fig. 5*A*) or mutant G93A SOD1 (Fig. 5*B*), respectively. Treatment of the cells with epoxomicin also increased wild-type and mutant SOD1 levels (Fig. 5*C* and supplemental Fig. S5). These results indicate that wild-type and mutant SOD1 are degraded by both macroautophagy and the proteasome in COS-7 cells. The results shown in Figs. 3*A* and 5*A* indicate that not only SOD1 without a tag but also HA-tagged SOD1 is degraded by macroautophagy.

The Contributions of the Proteasome Pathway and Macroautophagy to Mutant SOD1 Degradation Are Comparable—We then assessed the relative contributions of proteasomal degradation and macroautophagy to the clearance of mutant SOD1. As shown in Fig. 6*A*, 10 mM 3-MA entirely suppresses the (3-MA-sensitive) macroautophagy-mediated degradation of mutant SOD1. 1 μM epoxomicin also entirely suppresses the (epoxomicin-sensitive) proteasome-mediated degradation of

mutant SOD1 (Fig. 6*B* and supplemental Fig. S6). Therefore, we compared mutant G93A SOD1 levels in 1 μM epoxomicin-treated cells with that of 10 mM 3-MA-treated cells. The SOD1 protein level in 3-MA-treated cells was comparable with that of epoxomicin-treated cells (Fig. 6, *C–F*). An increased accumulation of mutant SOD1 was detected in cells cotreated with both inhibitors compared with that of 3-MA-treated cells or epoxomicin-treated cells (Fig. 6, *E* and *F*). These data further support the idea that mutant SOD1 proteins are degraded by both macroautophagy and the proteasome and indicate that, in these cells, the contribution of macroautophagy to mutant SOD1 clearance is approximately equal to that of the proteasome pathway.

Macroautophagy Reduces the Toxicity of Mutant SOD1—Previous studies have shown that mutant SOD1-expressing cells are more susceptible to cell death induced by proteasome inhibition (33). We examined whether inhibiting the macroautophagy-mediated degradation of mutant SOD1 could also induce cell death in Neuro2a cells using three different assays.

Degradation of Mutant SOD1 by Macroautophagy

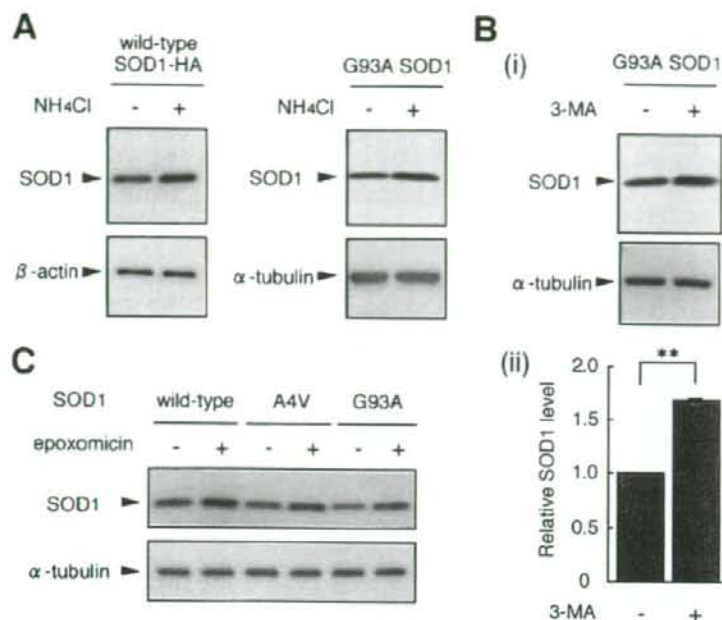


FIGURE 5. Mutant and wild-type SOD1 are degraded by both macroautophagy and the proteasome in COS-7 cells. *A*, COS-7 cells were transiently transfected with HA-tagged human wild-type SOD1 or G93A SOD1. 24 h after transfection, cells were incubated with or without 20 mM NH_4Cl for 24 h. Total cell lysates were analyzed by immunoblotting using anti-HA antibody or anti-SOD1 antibody. β -Actin and α -tubulin were used as loading controls. *B*, COS-7 cells transfected with G93A mutant SOD1 were incubated with or without 10 mM 3-MA in the presence of cycloheximide for 24 h. Total cell lysates were analyzed by immunoblotting using anti-SOD1 antibody (*i*). Levels of SOD1 were quantified by densitometry, and the levels are expressed as -fold level of SOD1 in cells with 3-MA over control. Data are presented as the means \pm S.E. ($n = 3$). ******, $p < 0.01$ (*ii*). *C*, COS-7 cells were transfected with wild-type or mutant A4V or G93A SOD1. 24 h after transfection, cells were incubated with or without 10 μM epoxomicin for 24 h. Total cell lysates were analyzed by immunoblotting.

For assessment of cell viability, we used the MTS assay and ATP assay, and for assessment of cell death, we used the lactate dehydrogenase release assay. In untreated differentiated Neuro2a cells, there was no statistically significant difference in cell viability or cell death among control cells, wild-type SOD1-expressing cells, and mutant SOD1-expressing cells (Fig. 7, A–C). However, when cells were treated with 3-MA, mutant SOD1-expressing cells showed significantly increased cell death and significantly decreased cell viability compared with control cells or wild-type SOD1-expressing cells (Fig. 7, D–F). When compared with cell death of 3-MA-untreated cells, cell death of 3-MA-treated cells was increased in mutant SOD1-expressing cells but not in cells with wild-type SOD1 (Fig. 7G). From these results, we conclude that macroautophagy reduces mutant SOD1-mediated toxicity in this cell model.

Inhibition of Macroautophagy Leads to Accumulation of both Detergent-soluble and Detergent-insoluble Mutant SOD1—Detergent-insoluble SOD1 proteins, aggregates, or inclusion bodies have been found in motor neurons in fALS patients (34), mouse models of fALS (35), and the cells transfected with mutant SOD1 (9, 36), although it is not clear whether these insoluble SOD1 proteins and aggregates are toxic because of conflicting results on the correlation between aggregate formation and cell death (36, 37). We investigated the effect of macroautophagy inhibition on the clearance of

nonionic detergent-soluble and -insoluble SOD1. The nonionic detergent-soluble and -insoluble fractions were subjected to SDS-PAGE following Western blotting. In agreement with a previous report (9), mutant SOD1 proteins exhibited increased nonionic detergent insolubility compared with wild-type SOD1 (Fig. 8B). The increased level of wild-type SOD1 compared with mutant in the detergent-soluble fraction (Fig. 8A) is probably due to the rapid turnover of mutant SOD1. Incubation with 3-MA increased monomer SOD1 levels in the detergent-soluble (Fig. 8A) and -insoluble fractions (Fig. 8B), suggesting that both detergent-soluble and -insoluble SOD1 are degraded by macroautophagy. Consistent with a previous report (9), we found SDS-resistant dimers and high molecular weight aggregates of mutant SOD1 in the detergent-insoluble fraction (Fig. 8C). These dimers and aggregates of mutant SOD1 were increased by 3-MA treatment (Fig. 8C), suggesting that insoluble aggregates of mutant SOD1 are also cleared by macroautophagy. The results

from Figs. 7 and 8 indicate that the accumulation of toxic mutant SOD1 proteins by macroautophagy inhibition leads to greater cell death.

DISCUSSION

Using inhibitors of macroautophagy and proteasomal degradation, we have shown that both wild-type and mutant SOD1 proteins are degraded by both pathways. Accumulating evidence has shown that mutant SOD1 is degraded by the ubiquitin-proteasome pathway (8, 9, 19). However, most of these studies have used lactacystin or a peptide aldehyde, both of which are not proteasome-specific inhibitors. Our data on the effect of the selective proteasome inhibitor epoxomicin also indicate that mutant SOD1 is degraded by the proteasome. Because wild-type SOD1 is not ubiquitinated by the ubiquitin ligases (10, 11), it has been proposed that wild-type SOD1 is not a substrate of the proteasome. However, a recent report has suggested that wild-type SOD1 can be degraded by the 20 S proteasome without ubiquitination (14). Moreover, we show here that epoxomicin treatment increases both overexpressed and endogenous wild-type SOD1 levels. Our data together with the previous reports support the idea that wild-type SOD1 is degraded by the 20 S proteasome in mammalian cells.

In this study, we demonstrated for the first time that macro-

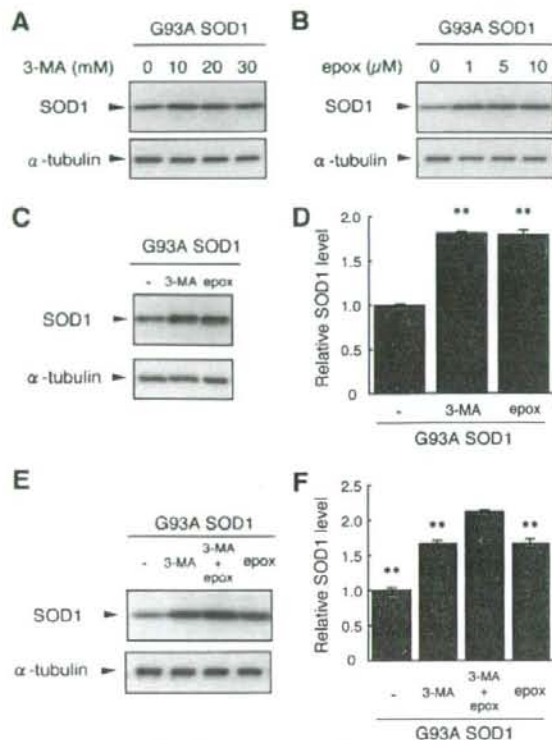


FIGURE 6. The contribution of macroautophagy to SOD1 clearance is comparable with that of the proteasome. *A*, Neuro2a cells transfected with mutant G93A SOD1 were incubated with or without 10, 20, or 30 mM 3-MA for 24 h. Total cell lysates were analyzed by immunoblotting. *B*, Neuro2a cells transfected with mutant G93A SOD1 were incubated with or without 1, 5, or 10 μ M epoxomicin (*epox*) for 24 h. Total cell lysates were analyzed by immunoblotting. *C* and *D*, Neuro2a cells transfected with mutant G93A SOD1 were incubated with or without 10 mM 3-MA or 1 μ M epoxomicin for 24 h. Total cell lysates were analyzed by immunoblotting (*C*). The relative level of mutant G93A SOD1 was quantified by densitometry. Data are presented as the means \pm S.E. ($n = 3$). **, $p < 0.01$ in comparison with control (analysis of variance with Dunnett's multiple comparison test). (*D*). *E* and *F*, COS-7 cells transfected with mutant G93A SOD1 were incubated with or without 10 mM 3-MA, 1 μ M epoxomicin, or both inhibitors (10 mM 3-MA and 1 μ M epoxomicin) in the presence of cycloheximide for 24 h. Total cell lysates were analyzed by immunoblotting (*E*). The relative level of mutant G93A SOD1 was quantified by densitometry. Data are presented as the means \pm S.E. ($n = 3$). **, $p < 0.01$ in comparison with 3-MA + epoxomicin (analysis of variance with Dunnett's multiple comparison test) (*F*).

autophagy is another pathway for degradation of wild-type and mutant SOD1. Our findings are consistent with a previous report that rat wild-type SOD1 is present in autophagosomes and lysosomes in rat hepatocytes (although they did not examine whether rat SOD1 was degraded by macroautophagy in those cells) (38). We propose that the contribution of macroautophagy to mutant SOD1 degradation is comparable with that of the proteasome pathway in the cell types we tested. Recent studies have demonstrated that transgenic mice with neuron-specific expression of mutant SOD1 do not exhibit an ALS-like phenotype (39, 40) and that neurodegeneration is delayed when motor neurons expressing mutant SOD1 are surrounded by healthy nonneuronal wild-type cells (41). In addition, Urushitani *et al.* (42) have shown that chromogranins promote secre-

Degradation of Mutant SOD1 by Macroautophagy

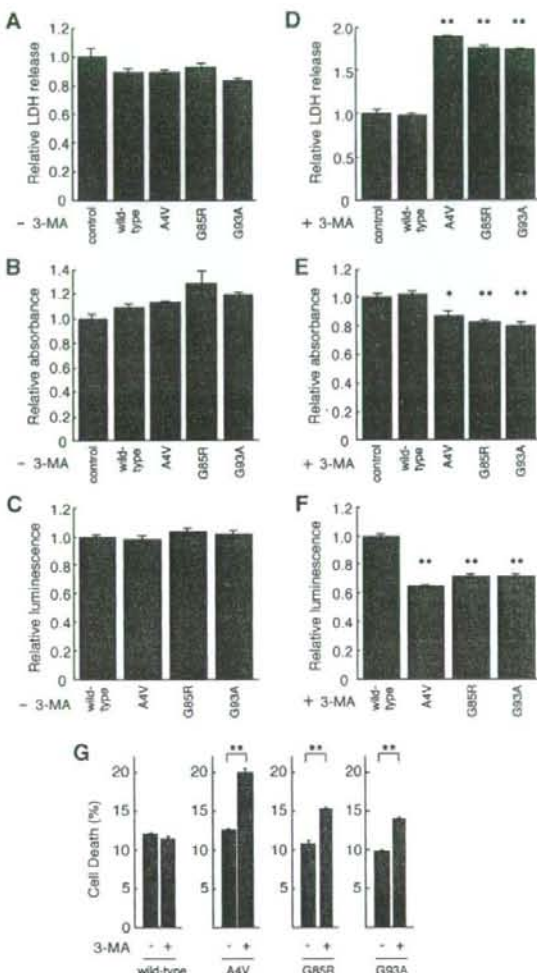


FIGURE 7. Macroautophagy inhibition causes mutant SOD1-mediated cell death. *A–G*, Neuro2a cells were transiently transfected with control empty vector (*A*, *B*, *D*, and *E*) or human SOD1 (wild type, A4V, G85R, or G93A). 24 h after transfection, cells were incubated in differentiation medium with (*D–G*) or without (*A–C* and *G*) 10 mM 3-MA for 24 h, and the lactate dehydrogenase release assay (*A*, *D*, and *G*), MTS assay (*B* and *E*), or ATP assay (*C* and *F*) were performed. The percentage of nonviable cells in each sample was calculated from the lactate dehydrogenase release assay (*G*). The experiment in *G* was performed independently of *A* and *D*. Data are expressed as the means \pm S.E. ($n = 4$ in *A*, *C*, *D*, *F*, and *G*; $n = 3$ in *B* and *E*). *, $p < 0.05$; **, $p < 0.01$ in comparison with control (*A*, *B*, *D*, and *E*) or with wild-type SOD1 (*C* and *F*) (analysis of variance with Dunnett's multiple comparison test). **, $p < 0.01$ (*G*; *t* test).

tion of mutant SOD1 from cells expressing the mutant protein, and they proposed that secreted mutant SOD1 can be toxic to neighboring cells. These studies strongly suggest that the expression of mutant SOD1 in nonneuronal cells may be involved in mutant SOD1-mediated neurotoxicity. In nonneuronal COS-7 cells, mutant SOD1 is also degraded by both the proteasome and macroautophagy (Fig. 5). Thus, not only the proteasome but also macroautophagy may play an important

Degradation of Mutant SOD1 by Macroautophagy

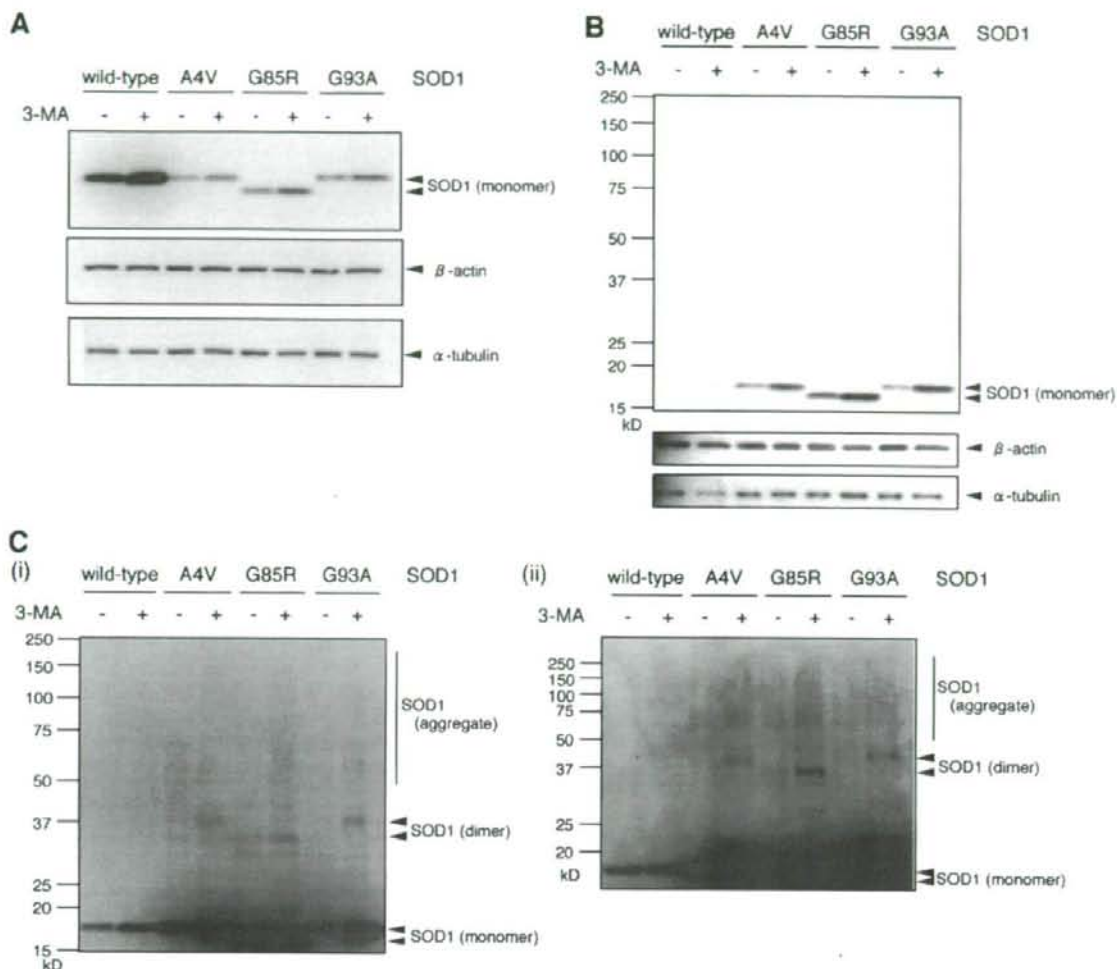


FIGURE 8. Inhibition of macroautophagy causes accumulation of both detergent-soluble and -insoluble mutant SOD1. A–C, Neuro2a cells were transiently transfected with human wild-type or mutant A4V, G85R, or G93A SOD1. 24 h after transfection, cells were cultured in differentiation medium with or without 10 mM 3-MA for 24 h. Triton X-100-soluble (A) and -insoluble (B and C) fractions were prepared and analyzed by immunoblotting using anti-SOD1 antibody. β -Actin and α -tubulin were used as loading controls. C (i), a longer exposure of B. C (j and ii), two different sets of experiments with longer exposure.

role in clearance of mutant SOD1 in fALS in nonneuronal cells as well as in neuronal cells.

It has been well established that mutant SOD1-mediated toxicity is caused by a gain of toxic function rather than the loss of SOD1 activity (1, 2). The appearance of mutant SOD1 aggregates in motor neurons in fALS patients and mouse models of fALS (34, 35) has suggested that aggregation has a role in neurotoxicity. However, conflicting results have been reported on the correlation between aggregate formation and cell death. A recent study has shown that the ability of mutant G85R and G93A SOD1 proteins to form aggregates correlates with neuronal cell death using live cell imaging techniques (36). Another report has concluded that aggregate formation of A4V and V148G SOD1 mutants does not correlate with cell death (37). These controversies also exist in other neurodegenerative dis-

eases (43–46). Our current data suggest that macroautophagy degrades toxic species of mutant SOD1 and that the accumulation of mutant SOD1 proteins leads to greater cell death. However, whether the toxic SOD1 species are monomers, oligomers, or aggregates cannot be determined from our study, because a variety of mutant SOD1 species, including detergent-soluble SOD1 monomers and detergent-insoluble monomers, dimers, and aggregates, were accumulated by macroautophagy inhibition (Fig. 8).

Our data show that macroautophagy reduces mutant SOD1-mediated toxicity and that induction of macroautophagy decreases mutant SOD1 protein levels. Niwa *et al.* (10) have shown that the ubiquitin ligase Dofrin ubiquitinates mutant SOD1 and prevents the neurotoxicity of mutant SOD1. Taken together, these data imply that macroautophagy inducers, acti-

vators of the ubiquitin-proteasome pathway, or a combination of the two have therapeutic potential for fALS. In conclusion, our results demonstrate that mutant SOD1 is degraded by at least two pathways, macroautophagy and the proteasome pathway, and that the clearance of mutant SOD1 by macroautophagy reduces its cell toxicity. These findings may provide insight into the molecular mechanisms of the pathogenesis of fALS.

Acknowledgments—We thank Dr. Ryosuke Takahashi (Kyoto University) and Dr. Makoto Urushitani (Laval University) for the gift of pcDNA3-hSOD1 (wild-type and mutant A4V, G85R, and G93A) plasmids, and Naoki Takagaki for the support in English.

REFERENCES

- Bruijn, L. I., Miller, T. M., and Cleveland, D. W. (2004) *Annu. Rev. Neurosci.* **27**, 723–749
- Cleveland, D. W., and Rothstein, J. D. (2001) *Nat. Rev. Neurosci.* **2**, 806–819
- Rosen, D. R., Siddique, T., Patterson, D., Figlewicz, D. A., Sapp, P., Hentati, A., Donaldson, D., Goto, J., O'Regan, J. P., Deng, H. X., Rahmani, Z., Krius, A., McKenna-Yasek, D., Cayabyab, A., Gaston, S. M., Berger, R., Tanzi, R. E., Halperin, J. J., Herzfeldt, B., Van den Bergh, R., Hung, W. Y., Bird, T., Deng, G., Mulder, D. W., Smyth, C., Laing, N. G., Soriano, E., Pericak-Vance, M. A., Haines, J., Rouleau, G. A., Gusella, J. S., Horvitz, H. R., and Brown, R. H., Jr. (1993) *Nature* **362**, 59–62
- Gurney, M. E., Pu, H., Chiu, A. Y., Dal Canto, M. C., Polchow, C. Y., Alexander, D. D., Caliendo, J., Hentati, A., Kwon, Y. W., Deng, H. X., Chen, W., Zhai, P., Sufit, R. L., and Siddique, T. (1994) *Science* **264**, 1772–1775
- Reaume, A. G., Elliott, J. L., Hoffman, E. K., Kowall, N. W., Ferrante, R. J., Siwek, D. F., Wilcox, H. M., Flood, D. G., Beal, M. F., Brown, R. H., Jr., Scott, R. W., and Snider, W. D. (1996) *Nat. Genet.* **13**, 43–47
- Goldberg, A. L. (2003) *Nature* **426**, 895–899
- Cuervo, A. M. (2004) *Trends Cell Biol.* **14**, 70–77
- Hoffman, E. K., Wilcox, H. M., Scott, R. W., and Siman, R. (1996) *J. Neurol. Sci.* **139**, 15–20
- Johnston, J. A., Dalton, M. J., Gurney, M. E., and Kopito, R. R. (2000) *Proc. Natl. Acad. Sci. U. S. A.* **97**, 12571–12576
- Niwa, J., Ishigaki, S., Hishikawa, N., Yamamoto, M., Doyu, M., Murata, S., Tanaka, K., Taniguchi, N., and Sobue, G. (2002) *J. Biol. Chem.* **277**, 36793–36798
- Miyazaki, K., Fujita, T., Ozaki, T., Kato, C., Kurose, Y., Sakamoto, M., Kato, S., Goto, T., Itoyama, Y., Aoki, M., and Nakagawara, A. (2004) *J. Biol. Chem.* **279**, 11327–11335
- Shringarpure, R., Grune, T., Mehilase, J., and Davies, K. J. (2003) *J. Biol. Chem.* **278**, 311–318
- Asher, G., Tsvetkov, P., Kahana, C., and Shaul, Y. (2005) *Genes Dev.* **19**, 316–321
- Di Noto, L., Whitson, L. J., Cao, X., Hart, P. J., and Levine, R. L. (2005) *J. Biol. Chem.* **280**, 39907–39913
- Komatsu, M., Waguri, S., Chiba, T., Murata, S., Iwata, J., Tanida, I., Ueno, T., Koike, M., Uchiyama, Y., Kominami, E., and Tanaka, K. (2006) *Nature* **441**, 880–884
- Hara, T., Nakamura, K., Matsui, M., Yamamoto, A., Nakahara, Y., Suzuki-Migishima, R., Yokoyama, M., Mishima, K., Saito, I., Okano, H., and Mizushima, N. (2006) *Nature* **441**, 885–889
- Komatsu, M., Waguri, S., Ueno, T., Iwata, J., Murata, S., Tanida, I., Ezaki, J., Mizushima, N., Ohsumi, Y., Uchiyama, Y., Kominami, E., Tanaka, K., and Chiba, T. (2005) *J. Cell Biol.* **169**, 425–434
- Ravikumar, B., Duden, R., and Rubinsztein, D. C. (2002) *Hum. Mol. Genet.* **11**, 1107–1117
- Urushitani, M., Kurisu, J., Tsukita, K., and Takahashi, R. (2002) *J. Neurochem.* **83**, 1030–1042
- Kabuta, T., Hakuno, F., Asano, T., and Takahashi, S. (2002) *J. Biol. Chem.* **277**, 6846–6851
- Lee, D. H., and Goldberg, A. L. (1998) *Trends Cell Biol.* **8**, 397–403
- Ostrowska, H., Wojcik, C., Wilk, S., Omura, S., Kozłowski, L., Stokłosa, T., Worowski, K., and Radziwon, P. (2000) *Int. J. Biochem. Cell Biol.* **32**, 747–757
- Meng, L., Mohan, R., Kwok, B. H., Eloffson, M., Sin, N., and Crews, C. M. (1999) *Proc. Natl. Acad. Sci. U. S. A.* **96**, 10403–10408
- Garcia-Echeverria, C. (2002) *Mini Rev. Med. Chem.* **2**, 247–259
- Qin, Z. H., Wang, Y., Kegel, K. B., Kazantsev, A., Apostol, B. L., Thompson, L. M., Yoder, J., Aronin, N., and DiFiglia, M. (2003) *Hum. Mol. Genet.* **12**, 3231–3244
- Cuervo, A. M., Stefanis, L., Fredenburg, R., Lansbury, P. T., and Sulzer, D. (2004) *Science* **305**, 1292–1295
- Kabeja, Y., Mizushima, N., Ueno, T., Yamamoto, A., Kirisako, T., Noda, T., Kominami, E., Ohsumi, Y., and Yoshimori, T. (2000) *EMBO J.* **19**, 5720–5728
- Webb, J. L., Ravikumar, B., Atkins, J., Skepper, J. N., and Rubinsztein, D. C. (2003) *J. Biol. Chem.* **278**, 25009–25013
- Blommaert, E. F., Luiken, J. J., Blommaert, P. J., van Woerkom, G. M., and Meijer, A. J. (1995) *J. Biol. Chem.* **270**, 2320–2326
- Gutierrez, M. G., Master, S. S., Singh, S. B., Taylor, G. A., Colombo, M. I., and Deretic, V. (2004) *Cell* **119**, 753–766
- Liang, X. H., Jackson, S., Seaman, M., Brown, K., Kempkes, B., Hibshoosh, H., and Levine, B. (1999) *Nature* **402**, 672–676
- Shimizu, S., Kanaseki, T., Mizushima, N., Mizuta, T., Arakawa-Kobayashi, S., Thompson, C. B., and Tsujimoto, Y. (2004) *Nat. Cell Biol.* **6**, 1221–1228
- Aquilano, K., Rotilio, G., and Ciriolo, M. R. (2003) *J. Neurochem.* **85**, 1324–1335
- Kato, S., Takikawa, M., Nakashima, K., Hirano, A., Cleveland, D. W., Kusaka, H., Shibata, N., Kato, M., Nakano, I., and Ohama, E. (2000) *Amyotroph. Lateral Scler. Other Motor Neuron Disord.* **1**, 163–184
- Bruijn, L. I., Becher, M. W., Lee, M. K., Anderson, K. L., Jenkins, N. A., Copeland, N. G., Sisodia, S. S., Rothstein, J. D., Borchelt, D. R., Price, D. L., and Cleveland, D. W. (1997) *Neuron* **18**, 327–338
- Matsumoto, G., Stojanovic, A., Holmberg, C. I., Kim, S., and Morimoto, R. I. (2005) *J. Cell Biol.* **171**, 75–85
- Lee, J. P., Gerin, C., Bindokas, V. P., Miller, R., Ghadge, G., and Roos, R. P. (2002) *J. Neurochem.* **82**, 1229–1238
- Rabouille, C., Strous, G. J., Crappo, J. D., Geuze, H. J., and Slot, J. W. (1993) *J. Cell Biol.* **120**, 897–908
- Pramatarova, A., Laganieri, J., Roussel, J., Brisebois, K., and Rouleau, G. A. (2001) *J. Neurosci.* **21**, 3369–3374
- Lino, M. M., Schneider, C., and Caroni, P. (2002) *J. Neurosci.* **22**, 4825–4832
- Clement, A. M., Nguyen, M. D., Roberts, E. A., Garcia, M. L., Boillee, S., Rule, M., McMahon, A. P., Doucette, W., Siwek, D., Ferrante, R. J., Brown, R. H., Jr., Julien, J. P., Goldstein, L. S., and Cleveland, D. W. (2003) *Science* **302**, 113–117
- Urushitani, M., Sik, A., Sakurai, T., Nukina, N., Takahashi, R., and Julien, J. P. (2006) *Nat. Neurosci.* **9**, 108–118
- Arrasate, M., Mitra, S., Schweitzer, E. S., Segal, M. R., and Finkbeiner, S. (2004) *Nature* **431**, 805–810
- Saudou, F., Finkbeiner, S., Devys, D., and Greenberg, M. E. (1998) *Cell* **95**, 55–66
- Schaffar, G., Breuer, P., Boteva, R., Behrends, C., Tsvetkov, N., Strippel, N., Sakahira, H., Siegers, K., Hayer-Hartl, M., and Hartl, F. U. (2004) *Mol. Cell* **15**, 95–105
- Nucifora, F. C., Jr., Sasaki, M., Peters, M. F., Huang, H., Cooper, J. K., Yamada, M., Takahashi, H., Tsuji, S., Troncoso, J., Dawson, V. L., Dawson, T. M., and Ross, C. A. (2001) *Science* **291**, 2423–2428



Dopaminergic neuronal loss in transgenic mice expressing the Parkinson's disease-associated UCH-L1 I93M mutant

Rieko Setsuie^{a,b,1}, Yu-Lai Wang^{a,1}, Hideki Mochizuki^{c,d}, Hitoshi Osaka^{a,e},
Hideki Hayakawa^c, Nobutsune Ichihara^f, Hang Li^a, Akiko Furuta^a, Yae Sano^{a,b},
Ying-Jie Sun^a, Jungkee Kwon^{a,g}, Tomohiro Kabuta^a, Kenji Yoshimi^d,
Shunsuke Aoki^a, Yoshikuni Mizuno^{c,d}, Mami Noda^b, Keiji Wada^{a,*}

^a Department of Degenerative Neurological Diseases, National Institute of Neuroscience, National Center of Neurology and Psychiatry, Kodaira, Tokyo 187-8502, Japan

^b Laboratory of Pathophysiology, Graduate School of Pharmaceutical Sciences, Kyushu University, Higashi-ku, Fukuoka 812-8582, Japan

^c Department of Neurology, Juntendo University School of Medicine, Bunkyo-ku, Tokyo 113-8421, Japan

^d Research Institute for Diseases of Old Age, Juntendo University School of Medicine, Bunkyo-ku, Tokyo 113-8421, Japan

^e Division of Neurology, Clinical Research Institute, Kanagawa Children's Medical Center, Yokohama 232-8555, Japan

^f Department of Anatomy, School of Veterinary Medicine, Azabu University, Sagami-ku, Sagami 229-8501, Japan

^g College of Veterinary Medicine, Chonbuk National University, 644-14 Duckjin-Ku, Jeonju 561-756, Republic of Korea

Received 14 March 2006; received in revised form 19 June 2006; accepted 11 July 2006

Available online 11 September 2006

Abstract

The I93M mutation in ubiquitin carboxyl-terminal hydrolase L1 (UCH-L1) was reported in one German family with autosomal dominant Parkinson's disease (PD). The causative role of the mutation has, however, been questioned. We generated transgenic (Tg) mice carrying human *UCHL1* under control of the *PDGF-B* promoter; two independent lines were generated with the I93M mutation (a high- and low-expressing line) and one line with wild-type human UCH-L1. We found a significant reduction in the dopaminergic neurons in the substantia nigra and the dopamine content in the striatum in the high-expressing I93M Tg mice as compared with non-Tg mice at 20 weeks of age. Although these changes were absent in the low-expressing I93M Tg mice, 1-methyl-4-phenyl-1,2,3,6-tetrahydropyridine (MPTP) treatment profoundly reduced dopaminergic neurons in this line as compared with wild-type Tg or non-Tg mice. Abnormal neuropathologies were also observed, such as silver staining-positive argyrophilic grains in the perikarya of degenerating dopaminergic neurons, in I93M Tg mice. The midbrains of I93M Tg mice contained increased amounts of insoluble UCH-L1 as compared with those of non-Tg mice, perhaps resulting in a toxic gain of function. Collectively, our data represent *in vivo* evidence that expression of *UCHL1*^{I93M} leads to the degeneration of dopaminergic neurons.

© 2006 Elsevier Ltd. All rights reserved.

Keywords: Ubiquitin carboxyl-terminal hydrolase L1; Animal model; Parkinson's disease; Dopaminergic neuron

1. Introduction

Parkinson's disease (PD) is the second most common human neurodegenerative disorder after Alzheimer's disease (AD) (Dauer and Przedborski, 2003; Vila and Przedborski, 2004). PD patients exhibit motor dysfunction, including slowed movement (bradykinesia), resting tremor, rigidity, and postural

instability (Dauer and Przedborski, 2003). The pathological basis of PD is the progressive loss of dopaminergic neurons in the substantia nigra pars compacta, giving rise to a decrease in dopamine content in the striatum (Dauer and Przedborski, 2003). Although most cases of PD are sporadic, studies of familial PD have provided accumulating evidence for the molecular mechanisms of PD. Thus far, at least six proteins have been identified to cause familial PD: α -synuclein (Chartier-Harlin et al., 2004; Farrer et al., 2004; Ibanez et al., 2004; Krüger et al., 1998; Polymeropoulos et al., 1997; Singleton et al., 2003), UCH-L1 (Leroy et al., 1998), parkin (Kitada et al., 1998), DJ-1 (Bonifati et al., 2003), phosphatase

* Corresponding author. Tel.: +81 42 346 1715; fax: +81 42 346 1745.

E-mail address: wada@ncnp.go.jp (K. Wada).

¹ These authors contributed equally to this work.

and tensin homolog induced kinase-1 (PINK1) (Valente et al., 2004), and leucine-rich repeat kinase-2 (LRRK2) (Paisan-Ruiz et al., 2004; Zimprich et al., 2004). α -Synuclein, UCH-L1 and LRRK2 are linked to the autosomal dominant form of PD, whereas parkin, DJ-1 and PINK1 are linked to the recessive form.

In 1998, UCH-L1 carrying an Ile to Met mutation at amino acid position 93 (I93M) was identified in one German family affected by autosomal dominant familial PD. UCH-L1, also known as PGP9.5, is an abundant protein in neuronal cells, comprising up to about 1–2% of total protein in the brain. Its function as de-ubiquitinating enzyme (Larsen et al., 1998; Wilkinson et al., 1989), ubiquitinating enzyme (Liu et al., 2002), de-neddylating enzyme (Hemelaar et al., 2004), and mono-ubiquitin stabilizer (Osaka et al., 2003) has been reported. *In vitro* analysis using recombinant human UCH-L1 indicated that I93M mutation results in the reduction of hydrolase activity of about 50% (Nishikawa et al., 2003). *Uchl1* gene deletion in mice, however, was reported to cause gracile axonal dystrophy (*gad*), a recessive neurodegenerative disease with distinct phenotype and pathological features from PD (Saigoh et al., 1999). Moreover, extensive analysis failed to find other PD patients with mutations in the *UCHL1* gene (Lincoln et al., 1999; Maraganore et al., 1999) and there was an incomplete penetrance in reported German family (Leroy et al., 1998). Thus, the correlation of I93M mutation and pathogenesis of PD was questioned.

To elucidate the pathological role of UCH-L1^{I93M} expression in the pathogenesis of PD, *in vivo*, we generated transgenic mice expressing human UCH-L1^{I93M}.

2. Experimental procedures

2.1. Generation of hUCHL1^{WT} and hUCHL1^{I93M} transgenic mice

We generated transgenes by cloning either the wild-type or I93M mutant human UCH-L1 cDNAs under the control of the human platelet-derived growth factor B chain (*PDGF-B*) promoter (Fig. 1A) (Sasahara et al., 1991). Sequences encoding *UCHL1* were amplified from a human brain cDNA library (Stratagene, La Jolla, CA) by PCR and subcloned into the *XhoI* and *NotI* sites of pCI-neo (Promega, Madison, WI). The I93M substitution was obtained using QuikChange (Stratagene). The 5' flanking region of the human *PDGF-B* chain gene was isolated from the human genomic DNA and inserted into the *BglII* and *XhoI* site of pCI-neo which results in the replacement of promoter from CMV to *PDGF-B*. The plasmid was linearized by digestion with *HindIII* and *AatII*. A 2 μ g/ml solution of the linearized plasmid of each transgene was then micro-injected into the pronuclei of newly fertilized C57BL/6J mouse eggs. Offspring were screened for the presence of the transgene by PCR of tail DNA using specific primers (forward: PD-UCH-2, 5'-GCACTCTCCCTTCTCCTTATA-3'; reverse: PD-UCH-5, 5'-CCTGTATGGCCTCATCTTTTC-3'). Expression of hUCH-L1^{I93M} in a low-expressing mouse line only occurred in male mice. Thus, all experiments were done using male heterozygous transgenic mice. Animal care and handling were in accordance with institutional regulations for animal care and were approved by the Animal Investigation Committee of the National Institute of Neuroscience, National Center of Neurology and Psychiatry, Tokyo, Japan which conforms the National Institute of Health guide for the care and use of Laboratory animals.

2.2. Quantitative RT-PCR analysis

Primers specific for mouse *Uchl1* (forward: mL1-7, 5'-CCTTGGTTTGACGCTTAGCA-3'; reverse: mL1-8, 5'-GGGCTGTAGAACGCAAGAAGA-3')

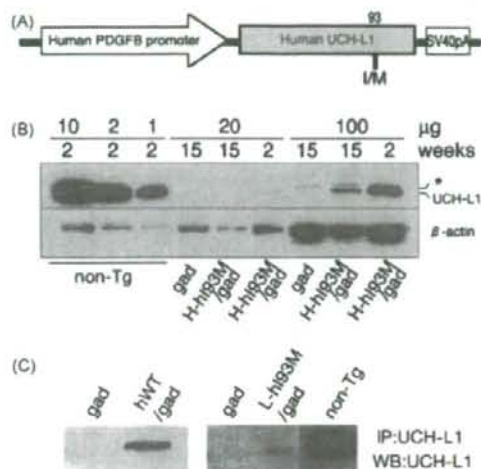


Fig. 1. Generation of transgenic mice expressing hUCH-L1^{WT} and hUCH-L1^{I93M}. (A) UCH-L1^{I93M} was constructed under control of the *PDGF-B* promoter, as depicted. (B) Immunoblotting analysis of endogenous mouse UCH-L1 and transgenic human UCH-L1 expression in mouse midbrain. To detect exogenous human UCH-L1 levels specifically, we generated transgenic mice in the *gad* background (H-hI93M/*gad*), which corresponds to the null mutant of *Uchl1*. Notice that the faint band corresponding to UCH-L1 is detected at 2 weeks of age when 20 μ g protein/lane was loaded for the detergent-soluble fraction of midbrain origin in H-hI93M/*gad* mice. When the applied protein was increased to 100 μ g/lane, UCH-L1 was easily detected at 2 weeks in H-hI93M/*gad* mice, and UCH-L1 levels markedly decreased by age 15 weeks. Faint bands indicated by the asterisk may correspond to UCH-L3, which cross-reacted with the UCH-L1 antibody when a large amount of protein was loaded per lane. (C) Immunoprecipitation analysis of exogenous human UCH-L1 in hWT/*gad* (left) and L-hI93M/*gad* (right) brains. Brain lysates from hWT/*gad* (left) or L-hI93M/*gad* (right) were both immunoprecipitated and detected using anti-UCH-L1 antibody. The band corresponding to the UCH-L1 can be found in both hWT/*gad* and L-hI93M/*gad* lysates but not in *gad* lysates indicating the exogenous human UCH-L1 expression.

and human *UCHL1* (forward: L1Tg-F2, 5'-TGGCAACTTCTCCTCTCGCA-3'; reverse: L1Tg-R2, 5'-ACAGCATTGTTCAGCATC-3') were designed, and SYBR Green-based real-time quantitative RT-PCR was performed using the ABI PRISM 7700 (Applied Biosystems, Foster City, CA) using total RNA from mouse brain ($n = 3$ for each line) (Aoki et al., 2002). GAPDH was used as an internal control.

2.3. Fractionation and immunoblotting and immunoprecipitation

For the immunoblotting of total UCH-L1, the soluble fraction in RIPA (20 mM Tris-HCl, pH 7.5; 0.1% SDS; 1.0% (w/v) Triton X-100; 1.0% sodium deoxycholate) with Complete EDTA-Free Protease Inhibitors (Roche, Basel, Switzerland) was extracted from H-hI93M/*gad* (high-expressing) UCH-L1^{I93M}-, *Uchl1*^{gad/gad}-, *gad* and non-Tg mouse midbrains. The extracted samples were loaded as indicated in Fig. 1.

For subfractionation, the cortex and hippocampus were removed from the midbrains of a H-hI93M mouse or a non-Tg littermate and bottom half under the aqueduct were used as the substantia nigra fraction. The fractionation method was modified from that of Kahle et al. (2001). Each sample was homogenized with 9 volumes of 5% SDS/TBS lysis buffer (50 mM Tris-HCl (pH 7.5), 150 mM NaCl, 5% SDS) with Complete EDTA-Free Protease Inhibitors using a 23G syringe. After three times of 10 s sonication, samples were ultra-centrifuged in 130,000 $\times g$ for 1 h, and the supernatant were pooled as 5% SDS fraction. The pellets were washed with 5% SDS/TBS solution once and further homogenized in 8 M urea/5% SDS/TBS lysis buffer

(8 M urea, 5% SDS, 50 mM Tris-HCl (pH 7.5), 150 mM NaCl) with 23G syringe. The resulting supernatant was used as 8 M urea/5% SDS fraction. The protein concentration was assessed by a DC-protein assay kit (Bio-Rad). 1.25 µg of 5% SDS fraction and 0.5 µg of 8 M urea/5% SDS fraction were subjected to SDS-PAGE using 15% gels (Perfect NT Gel; DRC, Tokyo, Japan). Anti-UCH-L1 (1:5000, RA95101; Ultraclone, Isle of Wight, UK) and anti-β-actin (1:5000, clone AC15; Sigma, St. Louis, MO) were used to detect each protein. Signals were detected using a chemiluminescent SuperSignal West Dura Extended Duration Substrate kit or West Femto Maximum Sensitivity Substrate kit (Pierce, Rockford, IL) and analyzed with a ChemImager (Alpha Innotech, San Leandro, CA). For the internal control of 8 M urea/5% SDS fraction, 1 µg protein were dot blotted to PVDF membrane and stained with Ponceau S staining (Rane et al., 2004). Statistical analyses were conducted using the two-tailed Student's *t*-test with total of four samples for each group.

For the immunoprecipitation, half of the brain (for hWT/gad) or mid-brain region (for L-h193M/gad) were homogenized in 2 ml ice-cold modified RIPA buffer (50 mM Tris-HCl, pH 7.4; 1% (w/v) Nonidet P40; 0.25% sodium deoxycholate; 150 mM NaCl; 1 mM EDTA) with Complete EDTA-Free Protease Inhibitors and centrifuged at 16,000 × *g* at 4 °C for 20 min. The protein concentration of the resulting supernatants was determined with the Protein Assay Kit (Bio-Rad, Hercules, CA). Immunoprecipitation was performed with a Seize X Mammalian Immunoprecipitation kit (Pierce, Rockford, IL) with some modifications. Briefly, 300 µg of protein was added to a 50 µl slurry of immobilized protein G cross-linked with rabbit polyclonal anti-human UCH-L1 (AB1716; Chemicon, Temecula, CA) or normal rabbit IgG and rotated at 4 °C overnight. The samples were then washed three times with 500 µl of 0.1B buffer (20 mM Tris-HCl, pH 8.0; 0.1 M KCl; 5 mM MgCl₂; 10% (w/v) glycerol; 0.1% (w/v) Tween 20; 10 mM β-mercaptoethanol). Elution of samples was performed by adding 20 µl of 5 × SDS-PAGE sample buffer, and samples were boiled at 100 °C for 5 min.

2.4. Immunohistochemistry, immunofluorescence and electron microscopy

Brain and peripheral (sciatic) nerve sections from 2-, 7- and 20-week-old mice were analyzed (*n* = 3 for each line) by immunocytochemistry as previously described (Wang et al., 2004; Watanabe et al., 1977) using antibodies to UCH-L1 (1:4000; RA95101; Ultraclone), TH (1:1000; Chemicon) and ubiquitin (1:1000; Sigma-Aldrich, St. Louis, MO). Antibody binding was detected with 3,3'-diaminobenzidine tetrachloride (DAB) or 3-amino-9-ethylcarbazole (AEC) as a peroxidase substrate or Alexa-488- or Alexa-568-conjugated secondary antibodies (Invitrogen, Carlsbad, CA). Sections were then counterstained with hematoxylin. Ultrastructural electron microscopic studies of the substantia nigra were performed as described (Watanabe et al., 1977) using midbrain sections.

2.5. MPTP treatment

For MPTP treatment, the mice received four injections of 30 mg/kg MPTP-HCl intraperitoneally (Research Biochemicals, Natick, MA) in saline at 24-h intervals (Mochizuki et al., 2001).

2.6. Tyrosine hydroxylase-positive cell counting and biochemical analysis

Samples for both histochemistry and biochemical analysis were obtained from the same mouse. Each animal was deeply anesthetized with pentobarbital and perfused transcardially with 10 ml of ice-cold phosphate-buffered saline, and the brain was removed and divided into forebrain and midbrain-hindbrain regions.

For the tyrosine hydroxylase (TH)-positive cell counting, midbrain-hindbrain was fixed with chilled 4% formaldehyde solution (pH 7.4). The procedure of TH-positive cell counting was described previously (Furuya et al., 2004) with minor modifications. Briefly, the substantia nigra was cut into serial sections (30 µm), and every third section was subjected to

immunostaining for TH using a polyclonal antibody to TH (a kind gift from I. Nagatsu, Fujita Health University, Aichi, Japan). The Vectorstain Elite ABC kit (Vector Labs, Burlingame, CA) was used for subsequent antibody detection with DAB as a peroxidase substrate. The number of viable TH-positive neurons was assessed by manual counting by a blind observer using coded slides (Furuya et al., 2004). The number of total neuronal cells outside the substantia nigra was counted after Bodian staining in the cerebral cortex (1 mm², seven regions per section), cerebellum (total of all lobules) and hippocampus (total number in CA1, CA2, CA3 and dentate gyrus). Statistical analysis were done by one-way ANOVA followed by post hoc test (Fisher's PLSD).

For the biochemical analysis, the striatum was quickly dissected from the forebrain, and the striatal tissue samples were weighed (~30 mg) and homogenized in 10 volumes (w/v) of ice-cold 0.05 M sodium acetate (pH 6.0). Homogenates were centrifuged (18,000 × *g*, 10 min at 4 °C), and the supernatant was frozen immediately on dry ice and stored frozen at -80 °C until use.

For the striatal dopamine measurement, supernatant (50 µl) from the striatal lysate was mixed with an equal volume of 0.2 M perchloric acid containing 0.2 mM EDTA and centrifuged (18,000 × *g*, 10 min at 4 °C), and the supernatant was applied to an HPLC system. Chromatographic separation was achieved using a C18 reversed-phase column (150 mm × 4.6 mm i.d., Model S-100; TOSOH, Tokyo, Japan). The mobile phase (50 mM citrate, 50 mM NaH₂PO₄, 0.1 mM EDTA, 4.36 mM 1-heptanesulfonate, 2.35% acetonitrile, 5.72% MeOH, pH 2.5) was pumped through the chromatographic system at a rate of 1.0 ml/min. A Coulochem electrode array system (ESA Inc., MA) with eight coulometric electrodes was used to quantify the eluted catecholamines and their metabolites. Statistical analysis was done by one-way ANOVA followed by post hoc test (Fisher's PLSD).

TH activity was assayed following the method of Hooper (1997) with minor modifications (Hooper et al., 1997; Naoi et al., 1988). The incubation mixture contained 50 µl of diluted sample and included the following components in a total volume of 200 µl: 0.2 M sodium acetate (pH 6.0), 0.2 M glycerol, 20,000 U/ml catalase, 1.0 mM 6-MPH4, 4.0 U/ml dihydropteridine reductase, 1 mM NADPH and 200 µM L-tyrosine. Incubations were carried out at 37 °C for 10 min in a shaking water bath. Reactions were terminated by adding 600 µl of ice-cold 0.33 M perchloric acid, 17 mM EDTA including 50 pmol of α-methyl DOPA as the internal standard. The L-DOPA produced was extracted onto alumina, and the catechols were eluted with 0.16 M acetic acid followed by 0.02 M phosphoric acid. A sample incubated on ice instead of 37 °C was used as a blank. The amount of L-DOPA was quantified with the HPLC system, as mentioned above. Statistical analysis was done by one-way ANOVA.

2.7. Silver staining

Sixty-micrometer brain sections from 12-week-old mice (*n* = 3 for each group) were stained using FD NeuroSilver kit (FD Neuro-Technologies, Catonsville, MD) according to the manufacturer's protocol to detect argyrophilic grain-positive degenerating neurons.

2.8. Behavioral tests

H-h193M mice and non-Tg littermates were used for all behavioral analyses. For the accelerated rota-rod test, 20–25-week-old mice were placed on the rod (Ohara, Japan) at a speed of 5 rpm, and the speed was accelerated to 50 rpm in 5 min. The length of time that each mouse was able to remain on the rod before falling was recorded. For the locomotor activity test, 11–13-week-old or 20–23-week-old mice were placed separately in a home cage 4 days before the beginning of analysis for habituation. Two to four mice were monitored at once for locomotor activity on the home cage monitor (Ohara, Japan) for 63 h beginning from 5:30 p.m. All mice were housed with a 12 h light/dark cycle, with the light cycle beginning at 8 a.m. The last 12 h of active night were used for the analysis. Mice were weighed after the analysis; there were no differences between the weights H-h193M and non-Tg mice (data not shown). Statistical analyses were conducted using the two-tailed Student's *t*-test.

3. Results

3.1. Generation of transgenic mice expressing human *UCHL1*^{H93M} in neurons of the substantia nigra

The human *PDGF-B* promoter was used to drive expression of the human *UCHL1* in Tg mice (Fig. 1A) (Sasahara et al., 1991). Germline transmission of *hUCHL1*^{H93M} was obtained in two independent Tg mouse lines (denoted L-hI93M and H-hI93M, where L and H denote low and high expression, respectively). Germline transmission of *hUCHL1*^{WT} was obtained in one Tg mouse line (denoted hWT). The levels of transgenic mRNA and endogenous *Uchl1* mRNA were assessed by quantitative RT-PCR using primers designed to amplify specifically the *UCHL1* transgene and mouse *Uchl1*, respec-

tively. The estimated relative expression of *UCHL1* among the transgenic lines was H-hI93M > hWT > L-hI93M. The ratio of endogenous mouse *Uchl1* transcripts to transgenic human *UCHL1* transcripts was 111 in H-hI93M, 739 in hWT and 6015 in L-hI93M ($n = 3$ for each line).

At the amino acid level, human and mouse UCH-L1 differ at only 11 discrete positions, and endogenous UCH-L1 is one of the most abundant protein in the brain. Therefore, we were not able to make distinction between the exogenous human UCH-L1 and endogenous mouse UCH-L1 in the brains of Tg mice (data not shown) using immunoblotting analysis with several antibodies against human UCH-L1 from different companies (Chemicon; UltraClone; Medac; Biogenesis). To ascertain the expression of transgene product, we used *gad* mice, which lack endogenous UCH-L1 (Saigoh et al., 1999). We mated mice

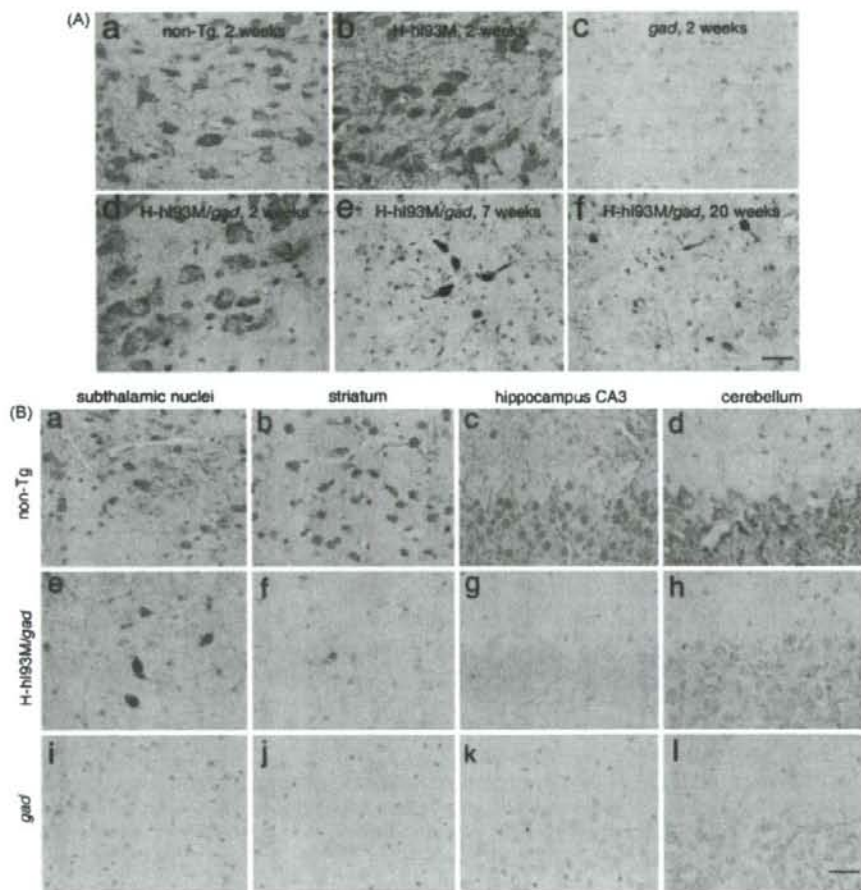


Fig. 2. Immunohistochemistry of UCH-L1 in coronal sections of the substantia nigra (A) and regions outside the substantia nigra (B) in H-hI93M, H-hI93M/*gad* and non-Tg mice. (A) Non-Tg mice (a), H-hI93M mice on a C57BL/6J background (b) and *gad* mice (c) at 2 weeks of age and H-hI93M/*gad* mice at 2 weeks (d), 7 weeks (e) and 20 weeks (f) of age. Neurons expressing UCH-L1 in the substantia nigra decreased in number and area, and densely stained neurons were observed in the aged substantia nigra. Scale bar: 30 μ m. (B) UCH-L1 immunohistochemistry of coronal sections at the level of the subthalamic nuclei (a, e, i), striatum (b, f, j), hippocampus CA3 (c, g, k) and cerebellum (d, h, l). Upper row (a–d), non-Tg mice; middle row (e–h), H-hI93M/*gad* mice; lower row (i–l), *gad* mice. All mice were examined at 2 weeks of age. Scale bar: 30 μ m.